

Extreme event probability estimation using PDE-constrained optimization and large deviation theory, with application to tsunamis*

Shanyin Tong[†], Eric Vanden-Eijnden[†], and Georg Stadler[†]

Abstract. We propose and compare methods for the analysis of extreme events in complex systems governed by PDEs that involve random parameters, in situations where we are interested in quantifying the probability that a scalar function of the system's solution is above a threshold. If the threshold is large, this probability is small and its accurate estimation is challenging. To tackle this difficulty, we blend theoretical results from large deviation theory (LDT) with numerical tools from PDE-constrained optimization. Our methods first compute parameters that minimize the LDT-rate function over the set of parameters leading to extreme events, using adjoint methods to compute the gradient of this rate function. The minimizers give information about the mechanism of the extreme events as well as estimates of their probability. We then propose a series of methods to refine these estimates, either via importance sampling or geometric approximation of the extreme event sets. Results are formulated for general parameter distributions and detailed expressions are provided when Gaussian distributions. We give theoretical and numerical arguments showing that the performance of our methods is insensitive to the extremeness of the events we are interested in. We illustrate the application of our approach to quantify the probability of extreme tsunami events on shore. Tsunamis are typically caused by a sudden, unpredictable change of the ocean floor elevation during an earthquake. We model this change as a random process, which takes into account the underlying physics. We use the one-dimensional shallow water equation to model tsunamis numerically. In the context of this example, we present a comparison of our methods for extreme event probability estimation, and find which type of ocean floor elevation change leads to the largest tsunamis on shore.

Key words. Extreme events, probability estimation, PDE-constrained optimization, large deviation theory, tsunamis.

AMS subject classifications. 65K10, 35Q93, 76B15, 60F10, 60H35

1. Introduction. Extreme events tend to occur rarely but are often consequential when they do. Examples from natural, social, and engineered systems include extreme weather patterns such as hurricanes or tornadoes, pandemics, the collapse of financial systems, cascading failures in power grids, and structural damage in dams or bridges. Estimating the probability of these events and uncovering the mechanisms behind their emergence can help inform strategies to mitigate their effects. However, given the complexity of their dynamics, it is typically unfeasible to calculate their probabilities explicitly. Monte Carlo methods are the standard approach to studying complex systems that include uncertainty. Unfortunately, these methods become inefficient to explore the

*Resubmitted March 2021.

Funding: S. T. and G. S. were partially supported by the US National Science Foundation (NSF) through grants DMS #1723211 and EAR #1646337, and by the SciDAC program funded by the U.S. Department of Energy, Office of Science, Advanced Scientific Computing Research, and Biological and Environmental Research Programs. E. V.-E. was supported in part by the NSF Materials Research Science and Engineering Center Program grant DMR #1420073, by NSF grant DMS #152276, by the Simons Collaboration on Wave Turbulence, grant #617006, and by ONR grant #N4551-NV-ONR.

[†]Courant Institute, New York University, New York, USA (shanyin.tong@nyu.edu, eve2@cims.nyu.edu, stadler@cims.nyu.edu).

probability tails associated with extreme events. The aim of this paper is to design efficient methods to estimate tail probabilities occurring in complex systems.

The methods we propose are meant to be generic and applicable to a broad class of problems. However, in this paper we use tsunamis as our main application example. Tsunami waves are generated by the displacement of a large amount of water due to a sudden and unpredictable elevation change in the ocean floor. This change, which occurs in conjunction with an earthquake, typically happens tens or hundreds of kilometers away from the coast line. As the tsunami waves travel to shore, they speed up in the deeper parts of the ocean and slow down in the shallower parts. This nonlinear interaction with the ocean floor combined with reflections from land features shape the tsunami waves that eventually reach the shore. To quantify the flooding-induced damage in locations of interest (e.g., cities or critical infrastructure), we use the average tsunami wave height in regions close to those locations. The random component in this system is the ocean floor elevation change. Given a distribution for possible elevation changes, we study the probability of observing extreme tsunamis close to the locations of interest. Additionally, we explore which type of elevation changes result in the largest tsunamis. The next section summarizes our approach, prior to a review of related work in this area.

1.1. Mathematical setup and methodological aspects. Following the strategy proposed in [14, 15], we use tools from large deviation theory (LDT) to connect probability estimation of extreme events with optimization. We assume that the randomness of the event under consideration can be captured by a parameter θ taking values in a Hilbert space Ω , e.g., $\Omega = \mathbb{R}^n$ or $\Omega = L^2(\mathcal{D})$ for a domain $\mathcal{D} \subset \mathbb{R}^n$, and whose statistics is specified by a probability measure μ . Given a parameter-to-event map $F : \Omega \rightarrow \mathbb{R}$ such that the larger $F(\theta)$, the rarer the event, we are interested in the probability

$$(1.1) \quad P(z) := \mathbb{P}(F(\theta) \geq z),$$

when z is large and hence $P(z) \ll 1$. In the applications we are interested in, $F(\theta)$ is of the form $F(\theta) = G(u(\theta))$, where G is some functional evaluated on the solution u of a (partial) differential equation (PDE), which we will denote by $e(u, \theta) = 0$: the parameter θ may enter this PDE for instance as a forcing, or as boundary or initial condition, and therefore its solution implicitly depends on θ , $u = u(\theta)$.

We will show that computation of the probability in (1.1) is aided by finding the most likely point (in the physical literature called *instanton*) $\theta^*(z)$ in the extreme event set $\Omega(z) := \{\theta \in \Omega : F(\theta) \geq z\}$, i.e., the solution of

$$(1.2) \quad \theta^*(z) = \operatorname{argmin}_{\theta \in \Omega(z)} I(\theta),$$

where I is the rate function from LDT defined in the subsequent sections and $\theta^*(z)$ is the global minimizer of I over the set $\Omega(z)$, which we assume to be unique. When $F(\theta) = G(u(\theta))$ where u solves $e(u, \theta) = 0$, (1.2) has the form of a PDE-constrained optimization problem. Under suitable assumptions on F and the distribution of θ to be detailed in section 2, the minimum $\theta^*(z)$ is attained on the boundary of $\Omega(z)$ and it can equivalently be characterized as solution of the problem

$$(1.3) \quad \theta^*(z) = \operatorname{argmin}_{\theta \in \Omega} I(\theta) - \lambda F(\theta)$$

for a specific parameter $\lambda > 0$. A variant of LDT then states that

$$(1.4) \quad \log P(z) \approx -I(\theta^*(z)) \quad \text{as } z \rightarrow \infty,$$

where “ \approx ” means that the ratio between the left and the right sides goes to 1 as $z \rightarrow \infty$. This shows that, by solving optimization problems of the form (1.2) (or equivalently (1.3) with appropriate $\lambda > 0$), we can estimate the log-asymptotic behavior of the probability $P(z)$ via (1.4). The details, along with the assumptions needed for (1.4) to hold, are given in section 2.

The next question we will address is how to get estimates of the probability (1.1) that are more accurate than (1.4). We show that this can be done in two ways. In section 3 we first propose an importance sampling (IS) method based on the optimizers $\theta^*(z)$ for different z . Compared to a vanilla Monte Carlo sampler, the sample variance of this IS does not include the term $\exp(-I(\theta^*(z)))$. This is a significant improvement as this term grows exponentially with the extremeness of events. This IS method allows asymptotically exact computation of $P(z)$.

The second way to improve upon (1.4) is to obtain an estimate that holds without the logarithm in this equation. That is, in section 4, we discuss how to find a function $C_0 : \mathbb{R} \rightarrow (0, \infty)$ such that

$$(1.5) \quad P(z) \approx C_0(z) \exp(-I(\theta^*(z))), \quad \text{as } z \rightarrow \infty.$$

The function $C_0(z) \geq 0$ is usually referred to as a “prefactor”. We will show that $C_0(z)$ can be calculated by exploiting the local derivative information at the optimizer $\theta^*(z)$ to construct the second-order approximation of the extreme set boundary $\partial\Omega(z)$. In the engineering literature, this approach is referred to as Second Order Reliability Method (SORM), and in section 4 we discuss conditions under which SORM is asymptotically exact, i.e., it leads to a prefactor $C_0(z)$ such that (1.5) holds. Additionally, we show how low-rank approximations can be used to compute SORM-based probabilities in high parameter dimensions. For completeness, in Appendix B we review another approach used by engineers, termed First Order Reliability Method (FORM), which gives another expression for $C_0(z)$: the FORM expression for $C_0(z)$ is simpler than that of SORM but we show that it is not asymptotically exact in general.

As an illustration, in sections 5 and 6 we apply our methodology to estimate the probability of extreme tsunami events on shore, which are caused by random, earthquake-induced elevation changes of the ocean floor described above. Here, the parameter-to-event map F involves the solution of a system of nonlinear PDEs, namely the shallow water equations. Since the random parameter θ in this problem is high-dimensional, solving the optimization problem (1.2) is challenging. We use an adjoint method for the efficient computation of derivatives of F with respect to θ and discuss the challenges of the resulting PDE-constrained optimization problem.

1.2. Related literature. Most methods for extreme event estimation are based on Monte Carlo (MC), Markov Chain Monte Carlo (MCMC) or importance sampling (IS) [37]. Standard MC sampling becomes impractical for extreme events due to the large number of required samples for unlikely events. MCMC sampling have similar shortcomings, but tailored variants such as Umbrella Sampling [46] can improve the estimation of tail probabilities. Importance sampling, [8, 31], decreases the required number of

samples by using proposal distributions that reduce the variance of the estimator. Recently proposed IS methods use ideas from Bayesian inference to find a maximum a posteriori (MAP) point and construct a Gaussian distribution centered at that point as IS proposal [42, 44, 52]. These methods require MAP points that lie in the pre-image of certain extreme events, and finding such events can be computationally extensive. In particular, the authors of [52] compute a Gaussian IS proposal by minimizing the Kullback-Leibler divergence to the ideal IS proposal. In [42], the authors propose to draw observation pairs from Rice's formula. Both methods rely on the linearity of the parameter-to-event maps and linearize them for nonlinear problems.

In this paper, we follow the approach proposed in [15] that takes the perspective of large deviation theory [16, 50] to estimate extreme event probabilities in system with random components and applies the resulting methods to quantify the probability of the occurrence of rogue waves [13, 14]. These papers solve an optimization problem that finds the most important point (also called instanton) in the extreme event set. This present paper uses a similar approach but generalize it in various directions, e.g., it provides prefactor estimators. In a related approach, the authors of [20, 43] search for initial condition leading to the highest growth in flow problems. This also requires solution of an optimization problem related to LDT optimization.

Probability estimation of extreme events is also of importance in engineering, e.g., for assessing the structural reliability of buildings or bridges [17]. Methods used in this context are based on the point with largest probability density (typically of a Gaussian distribution), combined with extreme event set approximations called First and Second Order Reliability Methods (FORM and SORM) [18, 41, 45]. These methods use a truncated Taylor expansion of the parameter-to-event map at the most probable point to estimate probabilities. Also IS methods based on the most probable point have been proposed [31, 45]. Our approach has similarities with these engineering methods, but uses instead the minimizer of the rate function from LDT, which describes the asymptotic behavior of the probability and can be used to design IS methods [19, 49]. Since the rate function of a Gaussian distribution is a multiple of its log-density, our methods generalize FORM and SORM, and provide theoretical justification for these approaches. Moreover, our methods apply to complicated dynamical systems (governed for instance by ODEs or PDEs) with high-dimensional parameters as they only require derivatives that can be computed efficiently using adjoint methods.

We use the methods we propose to estimate the probability of extreme tsunami waves on shore after sudden earthquake-induced ocean floor changes, which are modeled as random. As governing equations, we use the one-dimensional shallow water equations [35, 51], discretized with discontinuous-Galerkin finite elements [29]. To prevent the occurrence of shocks in these nonlinear hyperbolic equations, we add artificial viscosity [10]. This also provides justification to using the adjoint method to compute derivatives for optimization problems governed by hyperbolic equations [24, 48].

The proposed methods require the solution of optimization problems involving complex systems that are typically governed by PDEs. While the structure of these problems is similar to problems occurring in optimal control and inverse problems, the extreme event perspective suggests several novel research directions. First, it motivates to study new classes of governing equations, e.g., hyperbolic systems and their discretiza-

tion [24, 26, 27, 48, 53]. Second, it required to study and compute post-solution properties of minimizers, e.g., estimation of second derivatives as in Bayesian inference [1, 9] or parametric sensitivity analysis [25]. Third, as it is typically unknown when an extreme event will occur, it motivates further study of time-optimal control problems and their numerical solution in complex applications [21, 32].

1.3. Contributions and limitations. The main contributions of this work are as follows: (1) We present an extreme event probability estimation framework that exploits connections between probability estimation and PDE-constrained optimization, and apply it to a complex example problem. (2) We propose approaches to refine the asymptotic probability estimates from LDT by approximations of the extreme event sets. The computational cost of these approximations is independent of the extremeness of the events. (3) We show that importance sampling leveraging the LDT optimizers can lead to an exponential reductions of relative errors in all parameter directions. (4) As our tsunami application problem is governed by the 1D shallow water equations, we derive adjoint equations for this nonlinear hyperbolic conservation law and use them to efficiently compute gradients of the LDT objective.

Our work also has several limitations: (1) Most of the presented expressions for extreme event probability estimation are for an underlying Gaussian probability distribution. Possible generalizations depend on the probability measure and must be considered on a case-by-case basis. However, our explicit expressions apply to distributions that can be mapped to Gaussian distributions. (2) The proposed approach requires regularity properties, e.g., that the optimization problem has a unique solution and that the rate function of the parameter distribution is well-defined. Some properties of the parameter-to-event map F discussed in the next section can be difficult to verify a priori, but some may be verified a posteriori. (3) The tsunami model used in this work is one-dimensional, thus not allowing some of the complexity of a more realistic two-dimensional setup. However, our framework is generic and applies to more complex problems as long as derivatives of the objective with respect to the parameters are available. (4) We make some simplifying choices in the numerical scheme used for the shallow water equations, e.g., we use uniform time steps and a global Lax-Friedrichs flux. Some of these choices could be relaxed and while such a discussion is definitely interesting, it is beyond the scope of this paper.

1.4. Notation. Throughout the paper we repeatedly use asymptotic estimates. Thus, we introduce the following notation, where we consider the asymptotic parameter $s \rightarrow \infty$. Then, for $a(s), b(s) > 0$, we introduce the notation:

$$(1.6a) \quad a(s) \approx b(s) \quad \text{if} \quad \frac{a(s)}{b(s)} \rightarrow 1 \text{ as } s \rightarrow \infty,$$

$$(1.6b) \quad a(s) \lesssim b(s) \quad \text{if} \quad a(s) \leq b(s) \text{ for all } s, \text{ and } \frac{a(s)}{b(s)} \rightarrow 1 \text{ as } s \rightarrow \infty,$$

$$(1.6c) \quad a(s) \gtrsim b(s) \quad \text{if} \quad a(s) \geq b(s) \text{ for all } s, \text{ and } \frac{a(s)}{b(s)} \rightarrow 1 \text{ as } s \rightarrow \infty.$$

We commonly use multivariate Gaussian parameters in \mathbb{R}^n , $n \geq 1$. We say that a parameter θ follows $\theta \sim \mathcal{N}(\theta_0, C)$ when θ is a multivariate Gaussian parameter with mean

$\theta_0 \in \mathbb{R}^n$ and covariance matrix $C \in \mathbb{R}^{n \times n}$. Here, C is assumed to be symmetric and positive definite.

We regularly use a Hilbert space Ω and denote the corresponding inner product by $\langle \cdot, \cdot \rangle$ and the induced norm by $\|\cdot\|$. For the Euclidean inner product, we also use the vector notation $a^\top b = \langle a, b \rangle$ whenever convenient. Given a symmetric positive operator Q on Ω , we denote the weighted inner product by $\langle \cdot, \cdot \rangle_Q := \langle \cdot, Q \cdot \rangle$ and the induced norm by $\|\cdot\|_Q$.

2. Large deviation theory and optimization. Extreme event quantification aims at estimating the probability that a certain scalar quantity, which is a function of a random parameter θ , is at or beyond a threshold. In this section we summarize how ideas from LDT can be used to establish a formal connection between estimation of extreme events and optimization, loosely following [15]. We first show how the underlying distribution for the parameter θ defines the rate function $I : \Omega \mapsto \mathbb{R} \cup \infty$ occurring in the optimization problem (1.2).

For a parameter θ with probability distribution $\mu(\theta)$, the cumulant generating function $S(\eta)$ is the logarithm of the moment generating function of θ

$$(2.1) \quad S(\eta) = \log \mathbb{E} e^{\langle \eta, \theta \rangle} = \log \int_{\Omega} e^{\langle \eta, \theta \rangle} d\mu(\theta),$$

and we define $I : \Omega \rightarrow \mathbb{R}$ to be the Legendre transform of $S(\eta)$:

$$(2.2) \quad I(\theta) = \max_{\eta \in \Omega} (\langle \eta, \theta \rangle - S(\eta)).$$

We will be interested in problems in which $I(\theta)$ plays the role of the large deviation rate function, as obtained from Gartner-Ellis theorem when it applies [16], and will therefore refer to it as such. We note that $I(\theta)$ is convex by definition, and it can be computed explicitly for some distributions. For completeness, we derive it for multivariate Gaussian and exponential distributions in [Appendix A](#). In particular, we find that the rate function $I(\theta)$ of a multivariate Gaussian distribution is the negative log-probability density. Next, we present the principle that allows to relate constrained optimization over $I(\theta)$ to estimating probabilities.

2.1. Large deviation principle. Given a parameter $\theta \in \Omega$ with probability measure μ , and a parameter-to-event map $F : \theta \mapsto \mathbb{R}$, LDT relates the probability $P(z) = \mathbb{P}(F(\theta) \geq z)$ and the minimizer (1.2) of the LDT rate function $I(\theta)$ in (2.2). A sketch of this relation is shown in [Figure 1](#). We now provide a formal proof of the LDT result (1.4). This proof is based on the five assumptions in [15], which we recall and generalize to accommodate a more general class of extreme events sets $\Omega(z)$ (see [Assumption 4](#)). Moreover, we discuss what each assumption means for a multivariate Gaussian parameter distribution.

Assumption 1. There exists a finite z_0 such that the restriction of the map F to the preimage of the interval $(z_0, \infty) \subset \mathbb{R}$, i.e., to the set $F^{-1}((z_0, \infty)) \subset \Omega$, is differentiable with $\|\nabla F\| \geq K > 0$ for a suitable $K > 0$.

Assumption 2. The probability measure μ is such that the cumulant generating function $S(\eta)$ (2.1) exists for all $\eta \in \Omega$ and defines a differentiable function $S : \Omega \rightarrow \mathbb{R}$.

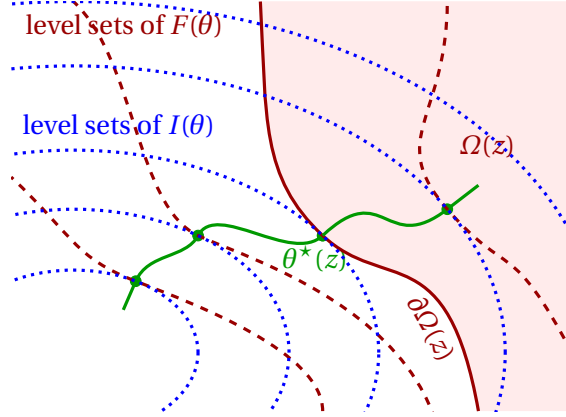


Figure 1. 2D illustration of level sets of the rate function $I(\cdot)$ and the extreme event sets $\Omega(z)$. For fixed z , $\theta^*(z)$ is the solution to an optimization problem and thus the gradients $\nabla F(\theta^*(z))$ and $\nabla I(\theta^*(z))$ align and after normalization equal to $\hat{n}^*(z)$. The path of the optimizers $\theta^*(z)$ for different z plays an important role in large deviation theory.

For a Gaussian parameter, $S(\eta) = \eta^\top \theta_0 + \frac{1}{2} \eta^\top C \eta$ as shown in (A.1), and thus this assumption is automatically satisfied. As in [15], Assumption 2 allows us to introduce the tilted measure $d\mu_\eta(\theta)$, which is used in the following assumptions:

$$(2.3) \quad d\mu_\eta(\theta) = \frac{e^{\langle \eta, \theta \rangle} d\mu(\theta)}{\int_{\mathcal{Q}} e^{\langle \eta, \theta \rangle} d\mu(\theta)} = e^{\langle \eta, \theta \rangle - S(\eta)} d\mu(\theta).$$

Assumption 3. There exists a finite z_0 and a constant K such that, $\forall z \geq z_0$, the rate function $I(\theta)$ has the unique global minimizer $\theta^*(z)$ in the set $\Omega(z) = \{\theta \in \Omega : F(\theta) \geq z\}$. In addition, the map $\theta^* : [z_0, \infty) \rightarrow \Omega$ is continuously differentiable and $I(\theta^*(\cdot))$ is strictly increasing with z with

$$(2.4) \quad I(\theta^*(z)) \rightarrow \infty \quad \text{and} \quad \|\nabla I(\theta^*(z))\| \geq K > 0 \quad \text{as} \quad z \rightarrow \infty.$$

For a Gaussian parameter, $I(\theta) = \frac{1}{2}(\theta - \theta_0)^\top C^{-1}(\theta - \theta_0)$, so $I(\theta^*(z)) \rightarrow \infty$ as long as $\|\theta^*(z)\| \rightarrow \infty$ as $z \rightarrow \infty$. Additionally, $\|\nabla I(\theta^*(z))\| = \|C^{-1}(\theta^*(z) - \theta_0)\| \geq \|\theta^*(z) - \theta_0\| / \lambda_{\max}(C^{-1}) \geq K > 0$ as long as $\|\theta^*(z) - \theta_0\| \geq K \lambda_{\max}(C^{-1})$ for $z \geq z_0$, where $\lambda_{\max}(C)$ is the largest eigenvalue of C . Thus, Assumption 3 is satisfied when $\|\theta^*(z)\| \rightarrow \infty$ as $z \rightarrow \infty$.

Since the rate function I is convex, Assumption 3 implies that $\theta^*(z) \in \partial\Omega(z)$ for $z > z_0$, i.e., we can replace (1.2) with

$$(2.5) \quad \theta^*(z) = \underset{\theta \in \partial\Omega(z)}{\operatorname{argmin}} I(\theta).$$

The corresponding Euler-Lagrange equation is

$$(2.6) \quad \nabla I(\theta^*(z)) = \lambda \nabla F(\theta^*(z)),$$

for some Lagrange multiplier $\lambda \in \mathbb{R}$. Following [15], if we define $\eta^*(z) := \nabla I(\theta^*(z))$, it is easy to see that the mean of $\mu_{\eta^*(z)}$ is $\theta^*(z)$. From the Legendre transform, this implies

that $\langle \eta^*(z), \theta^*(z) \rangle - S(\eta^*(z)) = I(\theta^*(z))$. Thus, we obtain an exact representation formula for the probability $P(z)$:

$$(2.7) \quad \begin{aligned} P(z) &= \int_{\Omega(z)} d\mu(\theta) = \int_{\Omega(z)} e^{S(\eta^*(z)) - \langle \eta^*(z), \theta \rangle} d\mu_{\eta^*(z)}(\theta) \\ &= e^{-I(\theta^*(z))} \int_{\Omega(z)} e^{-\langle \eta^*(z), \theta - \theta^*(z) \rangle} d\mu_{\eta^*(z)}(\theta). \end{aligned}$$

To prove the large deviation principle (1.4), we also need assumptions on $\Omega(z)$. Differently from [15], we avoid the assumption that $\Omega(z)$ is contained in the half-space

$$(2.8) \quad \mathcal{H}(z) := \{\theta : \langle \hat{n}^*(z), \theta - \theta^*(z) \rangle \geq 0\},$$

where $\hat{n}^*(z) = \nabla F(\theta^*(z)) / \|\nabla F(\theta^*(z))\| = \nabla I(\theta^*(z)) / \|\nabla I(\theta^*(z))\| = \eta^*(z) / \|\eta^*(z)\|$. Instead, we make a more general assumption.

Assumption 4. (Modified version of [15].) The set $\Omega(z)$ satisfies

$$(2.9) \quad \lim_{z \rightarrow \infty} \frac{\log \left(\int_{\Omega(z)} e^{-\langle \eta^*(z), \theta - \theta^*(z) \rangle} d\mu_{\eta^*(z)}(\theta) \right)}{I(\theta^*(z))} \leq 0.$$

This assumption relaxes the condition that $\Omega(z)$ is included in $\mathcal{H}(z)$, and expresses that the measure of $\Omega(z) \setminus \mathcal{H}(z)$ must be sufficiently small.

For a Gaussian parameter $\theta \sim \mathcal{N}(\theta_0, C)$, this assumption is related to the half-space approximation discussed later in this paper. Namely, the approximation (B.8) derived in [Appendix B](#) implies

$$(2.10) \quad \begin{aligned} \int_{\mathcal{H}(z)} e^{-\langle \eta^*(z), \theta - \theta^*(z) \rangle} d\mu_{\eta^*(z)}(\theta) &= (2\pi)^{-n/2} \det(C)^{-1/2} \int_{\mathcal{H}(z)} e^{I(\theta^*(z)) - I(\theta)} d\theta \\ &\leq \frac{1}{\sqrt{4\pi I(\theta^*(z))}}. \end{aligned}$$

Thus, we only need that

$$(2.11) \quad \lim_{z \rightarrow \infty} \frac{\log \left(\frac{1}{\sqrt{4\pi I(\theta^*(z))}} + \int_{\Omega(z) \setminus \mathcal{H}(z)} e^{-\langle \eta^*(z), \theta - \theta^*(z) \rangle} d\mu_{\eta^*(z)}(\theta) \right)}{I(\theta^*(z))} \leq 0,$$

which means that the part of $\Omega(z)$ not contained in $\mathcal{H}(z)$ must be sufficiently small. As further discussed in [subsection 4.1](#) later in this paper, if the set $\Omega(z)$ is contained in a paraboloid centered at $\theta^*(z)$, the curvature of that paraboloid must be in proper relation to the quadratic rate function. For details, we refer to the proof of [Theorem 4.2](#).

For the next assumption, which is needed for the lower bound, we first define $G(z, s) := \mu_{\eta^*(z)}(\Omega(z) \setminus \mathcal{H}(z, s))$ with

$$(2.12) \quad \mathcal{H}(z, s) := \{\theta : \langle \hat{n}^*(z), \theta - \theta^*(z) - \hat{n}^*(z)s \rangle \geq 0\}.$$

Assumption 5. There exists $s_1 > 0$ such that

$$(2.13) \quad \lim_{z \rightarrow \infty} \frac{\log G(z, s_1)}{I(\theta^*(z))} = 0.$$

This assumption ensures that the shape of $\Omega(z)$ does not degenerate as $z \rightarrow \infty$.

Theorem 2.1 (Large deviation principle). *Under Assumption 1 – Assumption 5, the following result, which is equivalent to (1.4), holds.*

$$(2.14) \quad \lim_{z \rightarrow \infty} \frac{\log P(z)}{I(\theta^*(z))} = \lim_{z \rightarrow \infty} \frac{\log \mu(\Omega(z))}{I(\theta^*(z))} = -1.$$

We note that this theorem is slightly different from a standard LDP [4, 7, 16, 50] since it involves taking the limit of the ratio of $\log P(z)$ and $I(\theta^*(z))$: in contrast a standard LDP would also establish how $I(\theta^*(z))$ grows as $z \rightarrow \infty$. Our result does not give this growth explicitly, and it has to be calculated numerically via estimation of $I(\theta^*(z))$ for large z . We will explain how to do so in section 3.

Proof. Assumption 1–Assumption 3 allow us to introduce the tilted measure and other terms discussed above. Applying Assumption 4 to (2.7), we find an upper bound for $P(z)$, namely

$$(2.15) \quad \lim_{z \rightarrow \infty} \frac{\log P(z)}{I(\theta^*(z))} = -1 + \lim_{z \rightarrow \infty} \frac{\log \left(\int_{\Omega(z)} e^{-\langle \eta^*(z), \theta - \theta^*(z) \rangle} d\mu_{\eta^*(z)}(\theta) \right)}{I(\theta^*(z))} \leq -1.$$

Splitting θ into the normal direction \hat{n}^* and orthogonal directions, i.e., $\theta = \theta^* + s\hat{n}^* + n^\top$, $\langle n^\top, \hat{n}^* \rangle = 0$, we have $\langle \eta^*(z), \theta - \theta^*(z) \rangle = \|\eta^*(z)\|s$, using the fact that $\eta^*(z)$ is parallel to \hat{n}^* from η^* 's definition. In addition, $G(z, \infty) = \mu_{\eta^*(z)}(\Omega(z))$ and $G(z, -\infty) = 0$, thus we can use $\partial_s G(z, s) ds$ as a new measure. As in [15], applying Fubini's theorem to (2.7) using the new measure $\partial_s G(z, s) ds$, followed by integration by parts, we obtain

$$(2.16) \quad \begin{aligned} P(z) &= e^{-I(\theta^*(z))} \int_{-\infty}^{\infty} e^{-\|\eta^*(z)\|s} \partial_s G(z, s) ds = e^{-I(\theta^*(z))} \int_{-\infty}^{\infty} e^{-\|\eta^*(z)\|s} \|\eta^*(z)\| G(z, s) ds \\ &\geq e^{-I(\theta^*(z))} \int_{s_1}^{2s_1} e^{-\|\eta^*(z)\|s} \|\eta^*(z)\| G(z, s) ds \geq e^{-I(\theta^*(z))} G(z, s_1) \int_{s_1}^{2s_1} d(-e^{-\|\eta^*(z)\|s}) \\ &= e^{-I(\theta^*(z))} G(z, s_1) e^{-\|\eta^*(z)\|s_1} (1 - e^{-\|\eta^*(z)\|s_1}) \geq e^{-I(\theta^*(z))} G(z, s_1) e^{-\|\eta^*(z)\|s_1} \frac{\|\eta^*(z)\|s_1}{1 + \|\eta^*(z)\|s_1}. \end{aligned}$$

Applying Assumption 5, we obtain the lower bound for $P(z)$

$$(2.17) \quad \lim_{z \rightarrow \infty} \frac{\log P(z)}{I(\theta^*(z))} \geq -1 + \lim_{z \rightarrow \infty} \frac{\log G(z, s_1) - \|\eta^*(z)\|s_1 - \log(1 + \|\eta^*(z)\|s_1)}{I(\theta^*(z))} = -1.$$

Combining (2.15) and (2.17) establishes (2.14) ■

2.2. The LDT optimization problem. We now discuss the optimization problem (1.2), whose solution is used in Theorem 2.1. Assumption 1 and Assumption 3 imply (2.5), i.e., the minimizer is attained on the boundary of $\Omega(z)$ and thus $F(\theta^*(z)) = z$. From the Karush-Kuhn-Tucker (KKT) conditions or the method of Lagrangian multipliers [5], and the regularity assumptions in Assumption 1, the minimizer $\theta^*(z)$ of (2.5) satisfies

$$(2.18) \quad \nabla I(\theta^*(z)) = \lambda^*(z) \nabla F(\theta^*(z)), \quad F(\theta^*(z)) = z,$$

where $\lambda^*(z) \in \mathbb{R}$ is a Lagrange multiplier. If F and I have second derivatives, then the second-order necessary conditions are:

$$(2.19) \quad \begin{aligned} & \forall \theta \in \Omega \text{ with } \langle \nabla I(\theta^*(z)), (\theta - \theta^*(z)) \rangle = 0 : \\ & \langle \theta, (\nabla^2 I(\theta^*(z)) - \lambda^*(z) \nabla^2 F(\theta^*(z))) \theta \rangle \geq 0. \end{aligned}$$

That is, the matrix $\nabla^2 I(\theta^*(z)) - \lambda^*(z) \nabla^2 F(\theta^*(z))$ is positive semidefinite in the tangent space of the constraint. The sufficient form of this second-order optimality condition, i.e., that the matrix is positive definite on the tangent space will play a role in [section 4](#), where we discuss approximations of extreme event probabilities that rely on the geometry of the extreme event set, and do not require sampling.

In practice, we are interested in solving the optimization problem (2.5) for different z . This can be done, for instance, by a projected gradient or Newton descent method. However, sometimes it is preferable to solve an unconstrained problem instead of (1.2) as discussed next.

2.3. Unconstrained formulation of LDT optimization problem. Here, we study when and in what sense the minimizers of the constrained optimization (1.2) can also be found as minimizers of the unconstrained optimization problem (1.3), that is,

$$(2.20) \quad \min_{\theta \in \Omega} H(\theta) \text{ where } H(\theta) := I(\theta) - \lambda F(\theta).$$

The function H is called the Hamiltonian, e.g., in [15]. Here, $\lambda > 0$ is considered to be a given constant. If we assume that the problem (2.20) has a unique global minimizer $\theta^*(\lambda)$ for every fixed $\lambda > 0$, then $\theta^*(\lambda)$ is also the global minimizer of (2.5) with $z = F(\theta^*(\lambda))$, i.e., of

$$(2.21) \quad \theta^*(\lambda) = \operatorname{argmin}_{\theta: F(\theta) = F(\theta^*(\lambda))} I(\theta).$$

This can be seen as follows: If the minimizer $\theta^*(z)$ of (2.5) with $z = F(\theta^*(\lambda))$ were not $\theta^*(\lambda)$, from uniqueness of $\theta^*(z)$ in [Assumption 3](#) we obtain $I(\theta^*(z)) < I(\theta^*(\lambda))$ and $F(\theta^*(z)) = F(\theta^*(\lambda))$, and thus $H(\theta^*(z)) < H(\theta^*(\lambda))$. This would contradict the assumption that $\theta^*(\lambda)$ is the unique minimizer of (2.20). Thus, under this assumption, the minimizer θ^* of the LDT problem (2.5) can also be computed by solving the unconstrained problem (2.20).

This provides us with an alternative approach to solve the LDT optimization problem (1.2) for various values of z . Namely, instead of considering a sequence of z 's in (1.2), one can consider a sequence of λ 's in (2.20). The solutions $\theta^*(\lambda)$ then correspond to the extremeness values $z = z(\lambda) := F(\theta^*(\lambda))$. Thus, $\lambda > 0$ can be used instead of the threshold z to control the extremeness of the event. Larger values of $F(\theta)$ correspond to extremer events. Such events can be found by increasing λ which puts more emphasis on the term involving F . Although the map $\lambda \rightarrow z(\lambda)$ is implicit, solving an unconstrained problem is often preferable to solving a constrained optimization problem. This is also the approach we take in [sections 5 and 6](#), where we describe our numerical example and present corresponding results.

In problems where the evaluation of F requires the solution of a PDE, (2.20) has the typical form of a PDE-constrained optimization problem, with the analogy that $I(\theta)$ is a

regularization term, and $F(\theta)$ involves the governing PDE. The existence and uniqueness of solutions for (2.20) depend on properties of $I(\cdot)$ and $F(\cdot)$, and must be studied on a case-by-case basis.

3. Probability estimation using optimization and sampling. The solutions $\theta^*(z)$ of (2.20) give the leading order contributions to the probability, i.e., the log-asymptotic approximation of $P(z)$ from the large deviation principle [Theorem 2.1](#). However, we still lack information regarding the omitted prefactor $C_0(z)$ in (1.5) since LDT only implies $\log(C_0(z))/I(\theta^*(z)) \rightarrow 0$ as $z \rightarrow \infty$. In this section we explore sampling methods to approximate $C_0(z)$.

3.1. Conventional Monte Carlo sampling. Although conventional Monte Carlo sampling is inefficient to study extreme events, we first summarize its properties to compare with other methods. The probability $P(z)$ in (1.1) can be written as the expectation of the indicator function for the set $\Omega(z)$. This implies an unbiased estimate of $P(z)$, [\[37\]](#),

$$(3.1) \quad P_N^{MC}(z) = \frac{1}{N} \sum_{k=1}^N \mathbb{1}_{\Omega(z)}(\theta_k),$$

where the θ_k 's are i.i.d. realizations (samples) from the distribution of θ , i.e., $\theta_k \sim \mu$.

The mean and the variance of the estimator in (3.1) are

$$(3.2) \quad \mathbb{E}_\mu [P_N^{MC}(z)] = P(z), \quad \mathbb{V}_\mu [P_N^{MC}(z)] = \frac{1}{N} [P(z) - P^2(z)].$$

Thus, the relative root mean square Error (RMSE) is

$$(3.3) \quad e_N^{MC}(z) = \frac{\sqrt{\mathbb{V}_\mu [P_N^{MC}(z)]}}{\mathbb{E}_\mu [P_N^{MC}(z)]} = \frac{1}{\sqrt{N}} \frac{\sqrt{P(z) - P^2(z)}}{P(z)} \approx \frac{1}{\sqrt{N}} \frac{1}{\sqrt{P(z)}},$$

where the last approximation holds for $z \rightarrow \infty$ as $P(z) \ll 1$, i.e., for extreme events when $P^2(z)$ is dominated by $P(z)$. Using (1.5), the relative RMSE is

$$(3.4) \quad e_N^{MC}(z) \approx \frac{1}{\sqrt{N}} \frac{1}{\sqrt{C_0(z)}} \exp\left(\frac{1}{2} I(\theta^*(z))\right),$$

indicating an exponential term that rapidly increases the number of samples needed.

For a Gaussian parameter distribution, this term can be computed explicitly using results detailed in [Appendix B](#). Denoting by $\theta^*(z)$ the solution of (2.5), we have $z = F(\theta^*(z))$ since the minimizer $\theta^*(z)$ lies on the boundary of $\Omega(z)$. Thus we can use the half-space approximation (B.8) to obtain, for $z \rightarrow \infty$ that

$$(3.5) \quad P(z) \approx (2\pi)^{-\frac{1}{2}} \frac{\exp(-I(\theta^*(z)))}{\sqrt{2I(\theta^*(z))}}, \quad \text{where} \quad I(\theta) = \frac{1}{2}(\theta - \theta_0)^T C^{-1}(\theta - \theta_0)$$

Hence, the relative RMSE of $P_N^{MC}(z)$ for events with $P(z) \ll 1$ becomes

$$(3.6) \quad e_N^{MC}(z) \approx \frac{1}{\sqrt{N}} \frac{1}{\sqrt{P(z)}} \approx \frac{1}{\sqrt{N}} [4\pi I(\theta^*(z))]^{\frac{1}{4}} \exp\left(\frac{1}{2} I(\theta^*(z))\right),$$

where compared to (3.4) we were able to replace the unknown prefactor with an expression involving the quadratic rate function $I(\theta^*(z))$, which satisfies $I(\theta^*(z)) \rightarrow \infty$ as $z \rightarrow \infty$ according to [Assumption 3](#).

3.2. Combining Monte Carlo and LDT rate using a constant prefactor. A simple method to estimate the prefactor $C_0(z)$ is assuming it to be a constant C_0 . Although standard MC sampling might not be effective to study extreme events, it is a reasonable method for moderately extreme events and can be combined with the rates from LDT optimization to compute probability estimates for more extreme events. That is, we determine a constant C_0 by fitting $\exp(-I(\theta^*(z)))$ to the MC results. Beside making the uncontrolled approximation that the prefactor is constant, the method has another shortcoming: it requires MC sampling to estimate the probability of moderately extreme events. In practice, one needs to choose a regime for fitting, i.e., use the MC estimate for somewhat extreme events that still have reasonable MC accuracy. Then, LDT can be used to provide the probability of more extreme events. This approach was used in [14, 15].

3.3. Importance sampling for Gaussian parameters. From (3.6) and (3.4), we know that the number of samples needed for the conventional MC method increases exponentially with z , i.e., as the events become more extreme. For Gaussian parameters, this can significantly be improved using importance sampling (IS).

For fixed $\lambda > 0$, we again denote the solution of (2.20) by θ^* , and compute $z := F(\theta^*)$. The IS method we propose uses a Gaussian proposal with centered at θ^* , as sketched in Figure 2. By inserting $\theta^* - \theta^*$, the probability $P(z)$ defined in (1.1) becomes

$$\begin{aligned}
 P(z) &= (2\pi)^{-n/2} \det(C)^{-1/2} \int_{\Omega(z)} e^{-\frac{1}{2} \|\theta - \theta^* + \theta^* - \theta_0\|_{C^{-1}}^2} d\theta \\
 (3.7) \quad &= e^{-\frac{1}{2} \|\theta^* - \theta_0\|_{C^{-1}}^2} \cdot (2\pi)^{-n/2} \det(C)^{-1/2} \int_{\Omega(z)} e^{-(\theta - \theta^*)^\top C^{-1} (\theta^* - \theta_0)} e^{-\frac{1}{2} \|\theta - \theta^*\|_{C^{-1}}^2} d\theta \\
 &= e^{-I(\theta^*)} \mathbb{E}_{\tilde{\mu}} \left[\mathbb{1}_{\Omega(z)}(\tilde{\theta}) \exp(-(\tilde{\theta} - \theta^*)^\top C^{-1} (\theta^* - \theta_0)) \right],
 \end{aligned}$$

where $\tilde{\theta} \sim \mathcal{N}(\theta^*, C)$ with probability measure $\tilde{\mu}$. The corresponding IS estimator is

$$(3.8) \quad P_N^{IS}(z) = e^{-I(\theta^*)} \frac{1}{N} \sum_{k=1}^N \left[\mathbb{1}_{\Omega(z)}(\tilde{\theta}_k) \exp(-(\tilde{\theta}_k - \theta^*)^\top C^{-1} (\theta^* - \theta_0)) \right],$$

where $\tilde{\theta}_k$ are independent samples from $\mathcal{N}(\theta^*, C)$.

Let us now compute mean, variance and the relative RMSE of this estimator. Using (3.7), the mean and the variance of the estimator $P_N^{IS}(z)$ are given by

$$\begin{aligned}
 (3.9) \quad \mathbb{E}_{\tilde{\mu}} \left[P_N^{IS}(z) \right] &= e^{-I(\theta^*)} \mathbb{E}_{\tilde{\mu}} \left[\mathbb{1}_{\Omega(z)}(\tilde{\theta}) \exp(-(\tilde{\theta} - \theta^*)^\top C^{-1} (\theta^* - \theta_0)) \right] = P(z), \\
 \mathbb{V}_{\tilde{\mu}} \left[P_N^{IS}(z) \right] &= e^{-2I(\theta^*)} \frac{1}{N} \mathbb{V}_{\tilde{\mu}} \left[\mathbb{1}_{\Omega(z)}(\tilde{\theta}) \exp(-(\tilde{\theta} - \theta^*)^\top C^{-1} (\theta^* - \theta_0)) \right].
 \end{aligned}$$

Since $\theta^* = \theta^*(z)$ is the solution of (2.5), (3.9) and the approximation (3.5) yields

$$(3.10) \quad \mathbb{E}_{\tilde{\mu}} \left[\mathbb{1}_{\Omega(z)}(\tilde{\theta}) \exp(-(\tilde{\theta} - \theta^*)^\top C^{-1} (\theta^* - \theta_0)) \right] = e^{I(\theta^*)} P(z) \approx (2\pi)^{-\frac{1}{2}} \frac{1}{\sqrt{2I(\theta^*(z))}},$$

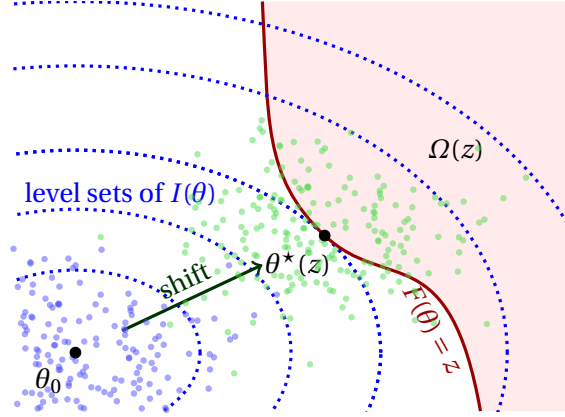


Figure 2. Sketch of importance sampling method based on shifting the mean θ_0 to the LDT-optimizer $\theta^*(z)$ for a specific z . Samples from the original distribution are shown in blue, and those used for IS are shown in green.

where $I(\theta^*) = \frac{1}{2}(\theta^* - \theta_0)^\top C^{-1}(\theta^* - \theta_0)$. The sample variance can be estimated as

$$\begin{aligned}
 & \mathbb{V}_{\tilde{\mu}} [\mathbb{1}_{\Omega(z)}(\tilde{\theta}) \exp(-(\tilde{\theta} - \theta^*)^\top C^{-1}(\theta^* - \theta_0))] \\
 (3.11) \quad &= \mathbb{E}_{\tilde{\mu}} [\mathbb{1}_{\Omega(z)}(\tilde{\theta}) \exp(-2(\tilde{\theta} - \theta^*)^\top C^{-1}(\theta^* - \theta_0))] - [e^{I(\theta^*)} P(z)]^2 \\
 &\approx (2\pi)^{-\frac{1}{2}} \frac{1}{2\sqrt{2I(\theta^*(z))}} - \left[(2\pi)^{-\frac{1}{2}} \frac{1}{\sqrt{2I(\theta^*(z))}} \right]^2 \lesssim (2\pi)^{-\frac{1}{2}} \frac{1}{2\sqrt{2I(\theta^*(z))}},
 \end{aligned}$$

where the last estimate holds for $z \rightarrow \infty$. Hence, the relative RMSE is

$$(3.12) \quad e_N^{IS}(z) = \frac{\sqrt{\mathbb{V}_{\tilde{\mu}} [P_N^{IS}(z)]}}{\mathbb{E}_{\tilde{\mu}} [P_N^{IS}(z)]} \approx \frac{1}{\sqrt{N}} \frac{\sqrt{(2\pi)^{-\frac{1}{2}} \frac{1}{2\sqrt{2I(\theta^*(z))}}}}{(2\pi)^{-\frac{1}{2}} \frac{1}{\sqrt{2I(\theta^*(z))}}} = \frac{1}{\sqrt{N}} [\pi I(\theta^*(z))]^{\frac{1}{4}}.$$

Thus, compared to (3.6), we removed the exponential term of (3.6) by using importance sampling with samples from $\mathcal{N}(\theta^*(z), C)$. This sampling error reduction holds for all directions. This IS method uses the covariance of the original distribution in the proposal distribution. Since we know the density decreases faster in the direction of $\nabla I(\theta^*)$, one may be able to modify the covariance matrix in this direction in order to decrease the variance of IS estimator, similar as in the IS method proposed in [52]. Generalizations of the presented approach to non-Gaussian distributions could rely on approximate mappings of the parameter distribution to a Gaussian distribution, or on Gaussian approximations of the distribution about an LDT optimizer.

4. Probability estimation using second-order approximation of extreme event set. Since $P(z) = \mu(\Omega(z))$, this probability can be computed by integrating the measure μ over the set $\Omega(z)$, provided we know or can approximate this set. Since evaluation of $F(\cdot)$ requires the solution of a PDE, $\Omega(z) = \{\theta : F(\theta) \geq z\}$ typically cannot be computed explicitly. However, we can construct an approximation of $\Omega(z)$ based on properties of the solution θ^* of (2.20), and integrate over this approximating set. For certain distributions, e.g., multivariate Gaussian distributions, this results in a computationally feasible

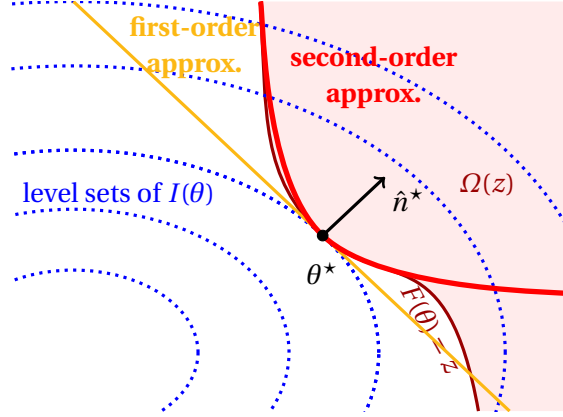


Figure 3. 2D illustration of the second-order approximation of the set $\Omega(z)$ for given z . These approximations exploit properties of the minimizer θ^* , the normal direction $\hat{n}^* := \nabla_{\theta} F(\theta^*) / \|\nabla_{\theta} F(\theta^*)\| = \nabla_{\theta} I(\theta^*) / \|\nabla_{\theta} I(\theta^*)\|$ and the curvature of $\partial\Omega(z)$ at θ^* . The first-order approximation is also given, its details are discussed in [Appendix B](#).

method. In this section, we discuss the approximation of $P(z)$ through integration over a second-order approximation of $\Omega(z)$, and provide explicit expressions for multivariate Gaussian parameters. For completeness, we present corresponding results based on a first-order approximation of Ω in [Appendix B](#). While this first-order approximation is easier to compute, it is not asymptotically exact in the sense of (1.5).

For the remainder of this section we consider a Gaussian parameter distribution $\theta \sim \mathcal{N}(\theta_0, C)$. In this case, the LDT minimizer θ^* is also the most probable point, since $\exp(-I(\theta))$ is the density of the Gaussian distribution up to a normalization constant; see [Example A.1](#). As will be shown in [subsection 4.1](#), one can derive explicit approximations of $P(z)$ using approximations of the extreme event set. As preparation step, we show how to transform the general Gaussian case to a standard normal distribution $\mathcal{N}(0, I)$. We also detail how the extreme event set, the rate function, and the parameter-to-event map are modified under this transformation.

Although all results in this section are presented in finite dimensions, we believe that they can be generalized to infinite dimensions, i.e., Gaussian random fields. In particular, if the expressions for the probabilities we find in [Theorem 4.2](#) converge as $n \rightarrow \infty$, they correspond to probabilities defined over an infinite-dimensional parameter space. In many cases, such a convergence follows from properties of the covariance operator of a Gaussian random field. However, a rigorous discussion of infinite-dimensional parameter spaces is beyond the scope this present paper.

We use the optimizer θ^* obtained by solving (2.20) for a fixed $\lambda > 0$. The corresponding event value is $z = F(\theta^*)$ as discussed in [subsection 2.2](#), i.e., $\theta^* = \theta^*(z)$. For simplicity of the notation, we drop the dependence of θ^* on z (and λ) in the subsequent derivations. We first define the affine transformation

$$(4.1) \quad \theta = A\xi + \theta_0, \quad A := C^{\frac{1}{2}}R,$$

where R is a rotation matrix such that $R^{\top}C^{-\frac{1}{2}}(\theta^* - \theta_0)$ is parallel to the first unit vector, i.e., only the first component of $R^{\top}C^{-\frac{1}{2}}(\theta^* - \theta_0)$ is nonzero and positive. The affine

transformation (4.1) maps the standard normal variable $\xi \sim \mathcal{N}(0, I_n)$ with measure μ^{SN} to a Gaussian variable $\theta \sim \mathcal{N}(\theta_0, C)$. Under this transformation, the rate function and parameter-to-event map become

$$(4.2) \quad \tilde{F}(\xi) := F(\theta) = F(A^{-1}\xi + \theta_0), \quad \tilde{I}(\xi) := I(\theta) = I(A^{-1}\xi + \theta_0) = \frac{1}{2}\|\xi\|^2.$$

The extreme event set $\Omega(z)$ is mapped to $\tilde{\Omega}(z) = \{\xi : \tilde{F}(\xi) \geq z\}$ and the derivatives become

$$(4.3) \quad \begin{aligned} \nabla_{\xi} \tilde{F}(\xi) &= A^{\top} \nabla_{\theta} F(\theta), & \nabla_{\xi}^2 \tilde{F}(\xi) &= A^{\top} \nabla_{\theta}^2 F(\theta) A, \\ \nabla_{\xi} \tilde{I}(\xi) &= A^{\top} \nabla_{\theta} I(\theta) = \xi, & \nabla_{\xi}^2 \tilde{I}(\xi) &= A^{\top} \nabla_{\theta}^2 I(\theta) A = I_n. \end{aligned}$$

The optimizer in the transformed system is $\xi^* = A^{-1}(\theta^* - \theta_0)$ and due to the definition (4.1), only the first component of ξ^* is nonzero and positive. The following Euler-Lagrange equation holds for the transformed functions \tilde{F} and \tilde{I} :

$$(4.4) \quad \nabla_{\xi} \tilde{I}(\xi^*) = \lambda \nabla_{\xi} \tilde{F}(\xi^*).$$

By construction, the normal direction at the optimal point ξ^* is :

$$(4.5) \quad \frac{\nabla_{\xi} \tilde{F}(\xi^*)}{\|\nabla_{\xi} \tilde{F}(\xi^*)\|} = \frac{\nabla_{\xi} \tilde{I}(\xi^*)}{\|\nabla_{\xi} \tilde{I}(\xi^*)\|} = \frac{\xi^*}{\|\xi^*\|} = e_1,$$

where e_1 the first unit vector. Finally, we introduce $P_n := [\mathbf{0}, I_{n-1}] \in \mathbb{R}^{(n-1) \times n}$, where $\mathbf{0} \in \mathbb{R}^{n-1}$ is the zero vector. This matrix represents a projection onto $E_1^{\perp} := \{e_1^{\perp} : \langle E_1^{\perp}, e_1 \rangle = 0\} = \{[0, \zeta], \zeta \in \mathbb{R}^{n-1}\}$, the hyperplane orthogonal to e_1 . Clearly, $P_n(E_1^{\perp}) = \mathbb{R}^{n-1}$ and every vector ξ in \mathbb{R}^n can be split uniquely as $\xi = [0, \zeta] + \xi_1 e_1$, where $\zeta = P_n(\xi)$.

4.1. Second-Order approximation of $\Omega(z)$. To approximate $\Omega(z)$, one can use a second-order approximation of $\partial\Omega(z)$. This is similar to the second-order reliability method (SORM) for Gaussian distributions in engineering [18], which replaces F in $F(\theta) \geq z$ by its second-order Taylor expansion at θ^* ,

$$(4.6) \quad F^{SO}(\theta) := F(\theta^*) + \langle \nabla_{\theta} F(\theta^*), \theta - \theta^* \rangle + \frac{1}{2} \langle \theta - \theta^*, \nabla_{\theta}^2 F(\theta^*) (\theta - \theta^*) \rangle.$$

Since $F(\theta^*) = z$, the corresponding estimate of $P(z)$ becomes

$$(4.7) \quad P^{SO}(z) = \mu(\mathcal{Q}(z)) = e^{-I(\theta^*(z))} \int_{-\infty}^{\infty} e^{-|\eta^*(z)|s} |\eta^*(z)| \mu_{\eta^*(z)}(\mathcal{Q}(z) \setminus \mathcal{H}(z, s)) ds,$$

where

$$(4.8) \quad \mathcal{Q}(z) := \{\theta : F^{SO}(\theta) \geq z\} = \left\{ \theta : \langle \nabla_{\theta} F(\theta^*), \theta - \theta^* \rangle + \frac{1}{2} \langle \theta - \theta^*, \nabla_{\theta}^2 F(\theta^*) (\theta - \theta^*) \rangle \geq 0 \right\}.$$

For a multivariate Gaussian parameter, it is possible to find an explicit approximation of $P^{SO}(z)$. First, we start with the standard normal case.

Lemma 4.1 (Measure of paraboloid for standard normal distribution). *Let $\xi \sim \mathcal{N}(0, I_n)$ in \mathbb{R}^n with measure μ^{SN} , $\xi^* = \|\xi^*\| e_1$ aligned with the first basis vector, and define the set $\tilde{\mathcal{Q}}_{\xi^*} := \{\xi : \langle e_1, \xi - \xi^* \rangle + \frac{1}{2} \langle \xi - \xi^*, H(\xi - \xi^*) \rangle \geq 0\}$, where $H \in \mathbb{R}^{n \times n}$ is a symmetric matrix such that $\langle \xi, (I - \|\xi^*\| H) \xi \rangle > 0$ for any $\xi \perp e_1$. Then, $\mu^{SN}(\tilde{\mathcal{Q}}_{\xi^*})$ satisfies*

$$(4.9) \quad \mu^{SN}(\tilde{\mathcal{Q}}_{\xi^*}) \approx (2\pi)^{-\frac{n}{2}} \frac{1}{\|\xi^*\|} e^{-\frac{1}{2} \|\xi^*\|^2} \prod_{i=1}^{n-1} [1 - \|\xi^*\| \lambda_i(H_1)]^{-\frac{1}{2}},$$

where the asymptotic estimate holds for $\|\xi^*\| \rightarrow \infty$. Here, $H_1 := P_n H P_n^\top \in \mathbb{R}^{(n-1) \times (n-1)}$ is the submatrix obtained by removing the first row and column of H , and $\lambda_i(\cdot)$ denotes the i -th eigenvalue.

Proof. First, we split ξ as $\xi = \xi^* + s e_1 + e_1^\perp$, $s \in \mathbb{R}$, $e_1^\perp \in E_1^\perp$ to obtain

$$(4.10) \quad \|\xi\|^2 = (\|\xi^*\| + s)^2 + \|\zeta\|_{\mathbb{R}^{n-1}}^2 \geq \|\xi^*\|^2 + 2s\|\xi^*\| + \|\zeta\|_{\mathbb{R}^{n-1}}^2,$$

where $\zeta := P_n(e_1^\perp) \in \mathbb{R}^{n-1}$. Since $\xi - \xi^* = s e_1 + e_1^\perp$ and e_1 and e_1^\perp are orthogonal, we can rewrite the term in the definition of $\tilde{\mathcal{Q}}_{\xi^*}$ as

$$(4.11) \quad \langle e_1, \xi - \xi^* \rangle + \frac{1}{2} \langle \xi - \xi^*, H(\xi - \xi^*) \rangle = s + \frac{s^2}{2} H_{11} + s \langle H_{2\dots n, 1}, \zeta \rangle_{\mathbb{R}^{n-1}} + \frac{1}{2} \langle \zeta, H_1 \zeta \rangle_{\mathbb{R}^{n-1}},$$

where $H_{11} \in \mathbb{R}$ is the $(1, 1)$ -entry of H , and $H_{2\dots n, 1} \in \mathbb{R}^{n-1}$ is the first column of H without the first component. Thus, we can compute the measure $\mu^{SN}(\tilde{\mathcal{Q}}_{\xi^*})$ using integration over e_1 and its orthogonal complement and use (4.10) and (4.11) to obtain

$$(4.12) \quad \mu^{SN}(\tilde{\mathcal{Q}}_{\xi^*}) = (2\pi)^{-\frac{n}{2}} \int_{s + \frac{s^2}{2} H_{11} + s \langle H_{2\dots n, 1}, \zeta \rangle_{\mathbb{R}^{n-1}} + \frac{1}{2} \langle \zeta, H_1 \zeta \rangle_{\mathbb{R}^{n-1}} \geq 0} e^{-\frac{1}{2} (\|\xi^*\| + s)^2 + \|\zeta\|_{\mathbb{R}^{n-1}}^2} d\zeta ds.$$

The integrand decays exponentially with increasing $|s|$ and $\|\zeta\|_{\mathbb{R}^{n-1}}$. However, for large $\|\xi^*\|$, the decay is (exponentially) faster in the direction e_1 (corresponding to s) than in the orthogonal direction e_1^\perp (corresponding to ζ) due to (4.10). Thus, the term $s^2 H_{11}$ in (4.11) is dominated by s and the term $s \langle H_{2\dots n, 1}, \zeta \rangle_{\mathbb{R}^{n-1}}$ by $\frac{1}{2} \langle \zeta, H_1 \zeta \rangle_{\mathbb{R}^{n-1}}$ as $\|\xi^*\| \rightarrow \infty$, which is why these terms can be neglected in the specification of the integration domain. As a consequence we obtain the asymptotic estimate

$$\mu^{SN}(\tilde{\mathcal{Q}}_{\xi^*}) \approx (2\pi)^{-\frac{n}{2}} \int_{s + \frac{1}{2} \langle \zeta, H_1 \zeta \rangle_{\mathbb{R}^{n-1}} \geq 0} e^{-\frac{1}{2} (\|\xi^*\| + s)^2 + \|\zeta\|_{\mathbb{R}^{n-1}}^2} d\zeta ds,$$

and using (4.10) and Fubini's theorem, we arrive at

$$\begin{aligned} \mu^{SN}(\tilde{\mathcal{Q}}_{\xi^*}) &\approx (2\pi)^{-\frac{n}{2}} \int_{s + \frac{1}{2} \langle \zeta, H_1 \zeta \rangle_{\mathbb{R}^{n-1}} \geq 0} e^{-\frac{1}{2} (\|\xi^*\|^2 + 2\|\xi^*\|s + \|\zeta\|_{\mathbb{R}^{n-1}}^2)} d\zeta ds \\ &= (2\pi)^{-\frac{n}{2}} e^{-\frac{1}{2} \|\xi^*\|^2} \int_{\mathbb{R}^{n-1}} e^{-\frac{1}{2} \|\zeta\|_{\mathbb{R}^{n-1}}^2} \left(\int_{-\frac{1}{2} \langle \zeta, H_1 \zeta \rangle_{\mathbb{R}^{n-1}}}^{\infty} e^{-\|\xi^*\|s} ds \right) d\zeta \\ &= (2\pi)^{-\frac{n}{2}} \frac{1}{\|\xi^*\|} e^{-\frac{1}{2} \|\xi^*\|^2} \int_{\mathbb{R}^{n-1}} e^{-\frac{1}{2} \langle \zeta, (I_{n-1} - \|\xi^*\| H_1) \zeta \rangle_{\mathbb{R}^{n-1}}} d\zeta. \end{aligned}$$

The assumption $\langle \xi, (I - \|\xi^*\|H)\xi \rangle > 0$ for any $\xi \perp e_1$ implies that $I_{n-1} - \|\xi^*\|H_1$ is positive, and thus we obtain that

$$\begin{aligned} \mu^{SN}(\tilde{\mathcal{Q}}_{\xi^*}) &\approx (2\pi)^{-\frac{1}{2}} \frac{1}{\|\xi^*\|} e^{-\frac{1}{2}\|\xi^*\|^2} \det[I_{n-1} - \|\xi^*\|H_1]^{-\frac{1}{2}} \\ &= (2\pi)^{-\frac{1}{2}} \frac{1}{\|\xi^*\|} e^{-\frac{1}{2}\|\xi^*\|^2} \prod_{i=1}^{n-1} [1 - \|\xi^*\| \cdot \lambda_i(H_1)]^{-\frac{1}{2}}. \quad \blacksquare \end{aligned}$$

Note that the condition $\langle \xi, (I - \|\xi^*\|H)\xi \rangle > 0$ in [Lemma 4.1](#) is equivalent to $1/\|\xi^*\| > \langle \xi, H\xi \rangle / \|\xi\|^2$. Geometrically, this condition means that the curvature of the centered circle through ξ^* must be an upper bound for the eigenvalues of H_1 , i.e., the projection of H onto the space orthogonal to e_1 . This circle is the level set through ξ^* of the rate function for the standard normal distribution. In the generalization of [Lemma 4.1](#) presented next, such a condition follows from the second-order optimality condition of the LDT-minimizer. This result uses the affine transformation (4.1) and applies [Lemma 4.1](#) to obtain an approximation of $P^{SO}(z)$ in (4.7).

Theorem 4.2 (Second-order approximation for general Gaussian distributions). *Let $\theta \sim \mathcal{N}(\theta_0, C)$, denote as $\theta^*(z)$ the optimizer with $\lambda > 0$ of (2.20), and define the rotation operator as in (4.1). Additionally, assume F is twice continuously differentiable and the minimizer θ^* satisfies that $C^{-1} - \lambda \nabla_{\theta}^2 F(\theta^*)$ is positive definite (as opposed to positive semi-definite), i.e., a second-order sufficient condition. Then, the second-order approximation $P^{SO}(z)$ defined in (4.7) can be approximated as*

$$(4.13) \quad P^{SO}(z) \approx \frac{(2\pi)^{-1/2}}{\sqrt{2I(\theta^*(z))}} e^{-I(\theta^*(z))} \prod_{i=1}^{n-1} \left[1 - \lambda \lambda_i \left(P_n R^\top (C^{\frac{1}{2}})^\top \nabla_{\theta}^2 F(\theta^*(z)) C^{\frac{1}{2}} R P_n^\top \right) \right]^{-\frac{1}{2}},$$

where the asymptotic estimate holds for $z \rightarrow \infty$. As before, $\lambda_i(\cdot)$ is the i -th eigenvalue and P_n is the projection onto the subspace orthogonal to the first basis vector.

Proof. Using (4.3), the set $\mathcal{Q}(z)$ defined in (4.8) is affinely transformed to

$$\begin{aligned} &\left\{ \xi : \langle A^{-\top} \nabla_{\xi} \tilde{F}(\xi^*), A\xi - A\xi^* \rangle + \frac{1}{2} \langle A\xi - A\xi^*, A^{-\top} \nabla_{\xi}^2 \tilde{F}(\xi^*) A^{-1} (A\xi - A\xi^*) \rangle \geq 0 \right\} \\ &= \left\{ \xi : \|\nabla_{\xi} \tilde{F}(\xi^*)\| \langle e_1, \xi - \xi^* \rangle + \frac{1}{2} \langle \xi - \xi^*, \nabla_{\xi}^2 \tilde{F}(\xi^*) (\xi - \xi^*) \rangle \geq 0 \right\} \\ &= \left\{ \xi : \langle e_1, \xi - \xi^* \rangle + \frac{1}{2} \langle \xi - \xi^*, H(\xi - \xi^*) \rangle \right\} = \tilde{\mathcal{Q}}_{\xi^*}, \end{aligned}$$

with $H = \nabla_{\xi}^2 \tilde{F}(\xi^*) / \|\nabla_{\xi} \tilde{F}(\xi^*)\|$. Thus, $P^{SO}(z) = \mu(\mathcal{Q}(z)) = \mu^{SN}(\tilde{\mathcal{Q}}_{\xi^*})$, for which we use [Lemma 4.1](#). Combining (4.3) and the Euler-Lagrange equation (4.4), we have

$$H = \frac{\nabla_{\xi}^2 \tilde{F}(\xi^*)}{\|\nabla_{\xi} \tilde{F}(\xi^*)\|} = \frac{\|\nabla_{\xi} \tilde{I}(\xi^*)\|}{\|\nabla_{\xi} \tilde{F}(\xi^*)\|} \frac{A^\top \nabla_{\theta}^2 F(\theta^*) A}{\|\xi^*\|}.$$

Thus, $I - \|\xi^*\|H = I - \lambda A^\top \nabla_{\theta}^2 F(\theta^*) A = R^\top (C^{\frac{1}{2}})^\top (C^{-1} - \lambda \nabla_{\theta}^2 F(\theta^*) C^{\frac{1}{2}} R)$ is positive, satisfying the assumption in [Lemma 4.1](#). Using this H and $\|\xi^*\| = \sqrt{2I(\theta^*)}$ from (4.2) in

Lemma 4.1, we obtain

$$P^{SO}(z) \approx \frac{(2\pi)^{-1/2}}{\sqrt{2I(\theta^*(z))}} e^{-I(\theta^*(z))} \prod_{i=1}^{n-1} [1 - \lambda \lambda_i (P_n A^\top \nabla_\theta^2 F(\theta^*) A P_n^\top)]^{-1/2}.$$

Using the definition of the linear operator A in (4.1) finishes the proof. \blacksquare

Note that (4.13) also holds when $P^{SO}(z)$ is replaced by $P(z)$. This follows from asymptotic expansions of multi-normal Laplace-type integrals [3, Chapter 8] and [6, Appendix I] using that F is twice differentiable, that $\theta^*(z)$ is the minimizer of $I(\theta)$ over $\Omega(z)$, and that $I(\theta^*(z)) \rightarrow \infty$ as $z \rightarrow \infty$ as assumed in Assumption 3. Thus, $P^{SO}(z)$ is an asymptotic approximation of $P(z)$ and we obtain an asymptotic approximation of the prefactor $C_0(z)$, i.e., $P(z) \approx C_0(z) \exp(-I(\theta^*(z)))$, as $z \rightarrow \infty$, where $C_0(z)$ is given by the right hand side in (4.13) neglecting the exponential term.

Note that the second-order sufficient condition in Theorem 4.2 is used to ensure that the right hand side in (4.13) is well-defined. Due to the occurrence of the projection P_n , this condition can be relaxed to $\langle \theta, (C^{-1} - \lambda \nabla_\theta^2 F(\theta^*)) \theta \rangle > 0$ for any θ satisfying $\langle \theta - \theta^*, C^{-1}(\theta^* - \theta_0) \rangle = 0$, i.e., to a second-order sufficient optimality condition for the constrained problem (2.5).

Compared to (4.13), the probability estimation based on the first-order (other than the second-order) approximation of $\Omega(z)$ is easier to compute. This approach, which is known in engineering as First-Order Reliability Method (FORM) is summarized in Appendix B. While it only requires θ^* , it does not provide a controllable approximation of the prefactor $C_0(z)$. In fact, FORM must be multiplied with a correction factor to obtain an asymptotically exact approximation. This leads to an alternative approach to approximate $P^{SO}(z)$ typically used in engineering. Namely, using the Euler-Lagrange equations (4.4) and the first-order approximation (B.8), we can reinterpret (4.13) as a refinement of $P^{FO}(z)$ with a correction term:

$$(4.14) \quad P^{SO}(z) \approx P^{FO}(z) \prod_{i=1}^{n-1} \left(1 + \sqrt{2I(\theta^*(z))} k_i\right)^{-1/2}.$$

Here, the k_i 's are the eigenvalues of $-P_n A^\top \nabla_\theta^2 F(\theta^*) A P_n^\top / \|A^\top \nabla_\theta F(\theta^*)\|$, i.e., the principle curvatures of F at θ^* . This is the formulation that is referred to as SORM in engineering, where the curvatures k_i are typically computed directly as detailed in [18]. However, we prefer the formulation (4.13) over (4.14) as it lends itself to approximating dominating eigenvalues with low-rank methods, which is particularly useful for high parameter dimensions. This approach, which to the best of our knowledge is novel, is presented next.

4.2. Low-rank approximation of covariance-preconditioned Hessian of F . A natural question is if the approximation for $P^{SO}(z)$ presented in Theorem 4.2 can be computed efficiently. In particular for problems where the parameter dimension n is large, and where the definition of F involves the solution of an expensive-to-solve PDE, computation of the Hessian matrix $\nabla_\theta^2 F(\theta^*)$ may be infeasible as computation of each of its columns requires at least two PDE solves. However, (4.13) shows that mostly the eigenvalues of $P_n R^\top (C^{\frac{1}{2}})^\top \nabla_\theta^2 F(\theta^*) C^{\frac{1}{2}} R P_n^\top$ that are significantly different from zero contribute to the product in (4.13) and thus to the estimate for $P^{SO}(z)$. Geometrically, these

eigenvalues correspond to directions in which the boundary $\partial\Omega(z)$ has large curvature. Additionally, these directions must correspond to large eigenvalues of the covariance matrix C , i.e., they must also be important for the underlying Gaussian distribution.

Using either the Lanczos algorithm or a randomized SVD [11, 28] allows to compute the dominant eigenvalues of $P_n R^\top (C^{\frac{1}{2}})^\top \nabla_\theta^2 F(\theta^*) C^{\frac{1}{2}} R P_n^\top$ without explicit construction of this matrix but only through application to vectors. The number of required matrix-vector applications for these methods is typically only slightly larger than the number of dominant eigenvalues. This number depends on properties of $\nabla_\theta^2 F(\theta^*)$ and C . While one cannot make general statements about the number of dominant eigenvalues, we show in [subsection 6.2](#) that for our tsunami example, this number is small, and is insensitive to $\lambda > 0$. Such a low-rank property is likely to also hold for other problems due to the structure of the matrix $(C^{\frac{1}{2}})^\top \nabla_\theta^2 F(\theta^*) C^{\frac{1}{2}}$, which we refer to as *covariance-preconditioned parameter-to-event Hessian*. A similar operator occurs in Bayesian inverse problems, where it is referred to as the prior-preconditioned misfit Hessian [9]. Dominant eigenvalues of $\nabla_\theta^2 F(\theta^*)$ correspond to directions with strong (either positive or negative) curvature of $\partial\Omega(z)$, i.e., their occurrence depends on the nonlinearity of the parameter-to-event map. Large eigenvalues of C correspond to directions with large variance, i.e., where the Gaussian measure has the majority of its mass. Only parameter directions that are important for $\nabla_\theta^2 F(\theta^*)$ and for C have eigenvalues with a large absolute value and thus contribute significantly to the right hand side in [\(4.13\)](#).

5. Application to extreme tsunami probability estimation. As our main application, we study earthquake-induced tsunamis and estimate the probability that they give rise to an extreme flooding event on shore. Tsunamis are caused by a sudden elevation change of the ocean floor after fast, and potentially complex, slip at the fault between two tectonic plates below the ocean floor. This slip process, also called dynamic rupture, is caused by stress buildup over years or decades. It typically occurs within seconds or, for the largest events a few minutes. In particular for large events, slip patterns are complex and difficult to predict. Hence, we model sudden ocean floor elevation changes as a random parameter field. Since the fault slip process is on a much faster time scale than the scale at which water waves travel, we do not include time dependence in this random process and consider the ocean floor elevation change as instantaneous. The map from these (random) parameters to the event, namely the average wave height in a region close to shore, is governed by the shallow water equation. Here, for simplicity, we use a one-dimensional shallow water model. The next subsections describe the shallow water equations and their discretization, modeling the distribution of the parameter field, the parameter-to-event map and the computation of its derivatives. Numerical results in which we study the performance of the proposed methods and the physics implications are presented in [section 6](#).

5.1. One-dimensional shallow water equations. To model tsunami waves, we use the one-dimensional shallow water equations [35] defined on a domain $\mathcal{D} = [a, b]$ for times $t \in [0, T_F]$. The domain represents a slice through the sea, that includes the shallow part near the shore and the part where the ocean floor elevation can change. We denote the horizontal fluid velocity as $u(x, t)$ and the height of water above the ocean floor by $h(x, t)$. The bathymetry $B(x)$ is the negative depth of the ocean at rest, i.e., $h(x, t) + B(x) =$

0 when the ocean is at rest. The shallow water equations in conservative form are

$$(5.1) \quad \begin{bmatrix} h \\ hu \end{bmatrix}_t + \begin{bmatrix} hu \\ hu^2 + \frac{1}{2}gh^2 \end{bmatrix}_x = \begin{bmatrix} 0 \\ -ghB_x \end{bmatrix},$$

where g is the gravitational constant and the subscripts t, x denote derivatives with respect to time and location. Introducing the variable $v := hu$ and augmenting (5.1) with initial and boundary condition leads to

$$(5.2a) \quad h_t + v_x = 0 \quad \text{on } \mathcal{D} \times [0, T_F],$$

$$(5.2b) \quad v_t + \left(\frac{v^2}{h} + \frac{1}{2}gh^2 \right)_x + ghB_x = 0 \quad \text{on } \mathcal{D} \times [0, T_F],$$

$$(5.2c) \quad h(x, 0) = -B_0(x), \quad v(x, 0) = 0 \quad \text{for } x \in \mathcal{D},$$

$$(5.2d) \quad v(a, t) = v(b, t) = 0 \quad \text{for } t \in [0, T_F].$$

Here, the initial condition (5.2c) assumes that the water is at rest. It can be verified that if $B = B_0$, $h = -B_0$ and $v = hu = 0$ for all times. However, any change in the bathymetry B results in a nonzero solution. This is the main mechanism that generates tsunami waves. Note that this form of the shallow water equations only allows to incorporate the vertical bathymetry change $B - B_0$. Earthquakes also alter the horizontal component of the bathymetry, but most likely this does not have a large effect on tsunami waves. The reflective boundary conditions (5.2d) are not physically accurate, but we assume that the boundary is far enough from the region where the tsunami wave is generated or measured such that unphysical reflections are not relevant. For a discussion on different boundary conditions for the shallow water equations, we refer to [51].

The domain we use for our tsunami model problem is shown in Figure 4. This setup is inspired by the 2011 Tohoku-Oki earthquake and tsunami [22]. The geometry represents a two-dimensional slice with a bathymetry that models the continental shelf and the pacific ocean to the east of Japan. We also use a similar slip mechanism as occurred in the Tohoku-Oki earthquake, as discussed next.

5.2. Modeling random parameter field B using subduction physics. The bathymetry $B(x)$, whose derivative enters in the right hand side of (5.2), changes during an earthquake as a result of slip between plates under the ocean floor. Since details of this slip process are difficult to predict, we model the slip as a random process, and thus also the bathymetry field B is random. Since B enters in the shallow water equations (5.2), the (space and time-dependent) solutions h and v are random and hence also the event objective we will specify in subsection 5.3 is a random variable.

The relation between slip under the sea floor and the resulting bathymetry change typically assumes that the earth's solid crust behaves like a linear elastic material. The commonly used Okada model [40] assumes a finite number of slip patches in a fault under the ocean floor, and evaluates expressions for a linear elastic material to compute the induced bathymetry change. We assume 20 slip patches and model each of the uncertain slips of fault pairs as independent Gaussian random parameter with mean zero and a standard deviation of 10m. We assume the slip to be along the down-dip direction, i.e., a positive slip value means that the overriding plate (i.e., the sea floor) moves downwards

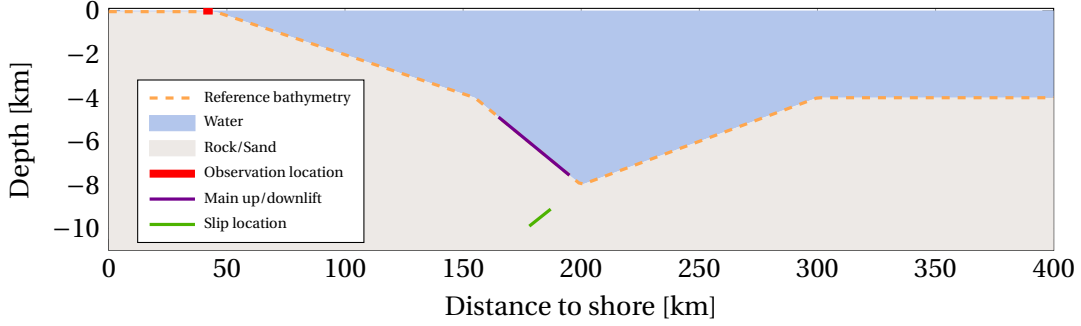


Figure 4. Problem setup inspired by Tohoku-Oki 2011 earthquake/tsunami. Bathymetry changes (area in purple) are modeled as resulting from 20 randomly slipping patches in the slip region (in green, with end points $(178\text{km}, -9.9\text{km})$ and $(187\text{km}, -9.1\text{km})$) using the Okada model. The event we observe is the average wave height in the interval $[40\text{km}, 44\text{km}]$ close to shore (shown in red), where the water depth at rest is 50m.

along the fault while a negative value means it is moving upwards. In this work we use a centered Gaussian slip distribution, which is a simplification as realistic earthquake slips are typically negative since they are caused by a sudden stress release. We refer to [23, 36] for more realistic slip distribution models, which we are currently incorporating into our framework. The Okada model is defined for three-dimensional sea floor deformations. By assuming that the width of each patch is infinite and extracting the deformation in the direction of the slice plane, we adopt the Okada implementation [2] to our two-dimensional geometry. The model assumes that the crust has a Poisson's ratio of $\nu = 0.25$, which is the only elasticity parameter that plays a role in the Okada model. The linear relationship between skip patches and bathymetry change results in

$$(5.3) \quad B(x) = B_0(x) + (OS)(x) \text{ with } S = (s_1, \dots, s_{20})^\top \text{ and } (OS)(x) := \sum_{i=1}^{20} s_i O_i(x),$$

where O_i is the bathymetry change due to the i -th slip patch, and $s_i \sim \mathcal{N}(0, 10)$. Hence

$$(5.4) \quad B \in \mathcal{B} := \left\{ B_0(x) + \sum_{i=1}^{20} s_i O_i(x) : s_i \in \mathbb{R} \right\}.$$

Random draws of the bathymetry change $B - B_0$ are shown in Figure 5. While the slips are independent, the bathymetry samples are smooth. This is due to properties of linear elasticity, i.e., rough boundary conditions on one part of the boundary result in a smooth displacement field on a different part of the boundary. Note also that all random samples of $B - B_0$ yield positive *and* negative elevation changes as typically also found in observations [22]. This is due to the fact that slip at the fault zone is tangential and thus leads to elastic compression in parts of the elastic domain and to extension in other parts.

Since the transformation (5.3) between slips and the bathymetry change is linear, B is a Gaussian random field with mean B_0 and covariance induced by the slip covariance matrix $C_s := 100I_{20}$. The rate function I for a bathymetry $B \in \mathcal{B}$ with coefficient vector $S \in \mathbb{R}^{20}$ is

$$(5.5) \quad I(B) = \frac{1}{2} S^\top C_s^{-1} S =: \frac{1}{2} \langle\langle B - B_0, B - B_0 \rangle\rangle_{C_s}.$$

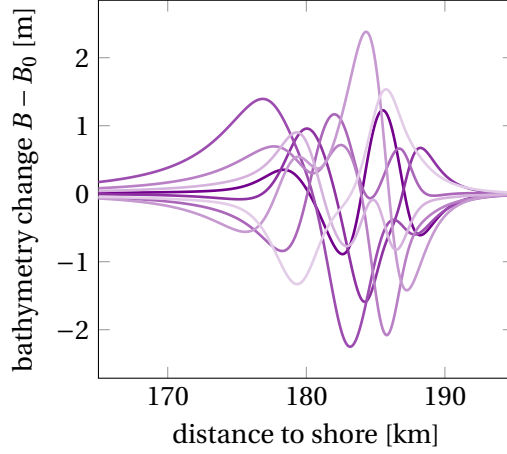


Figure 5. Samples from the bathymetry change distribution computed from the Okada model with 20 slip fault pairs under the ocean floor. Shown is the vertical ocean floor displacement. Each slip is independent with mean zero and standard deviation of 10m. The main part of the ocean floor where bathymetry change arises is highlighted in purple in Figure 4.

5.3. Measuring tsunami size close to shore. After discussing the governing equations and the parameter distribution for B , it remains to define how we measure events. Namely, to measure the size of a tsunami close to shore, we average the wave height ($h + B_0$) in the area $[c, d]$. This area is assumed to be sufficiently far away from where the main bathymetry change occurs such that we can consider $h + B_0$ rather than $h + B$. Hence, for a measurement time $t \in [0, T_F]$, we define f^{ob} as

$$(5.6) \quad f^{ob}(h, v; B, t) := \int_c^d [h(x, t) + B_0(x)] dx := \frac{1}{|d - c|} \int_c^d [h(x, t) + B_0(x)] dx,$$

where h and v are the solutions of shallow water equations (5.2) for given B , and f_c^d is the average of the integral over $[c, d]$. Since we do not know exactly at what time t the tsunami wave is close to shore, we take the maximum over the time interval, resulting in the parameter-to-event map $F : B \mapsto \bar{F}(h(B), v(B); B)$, where \bar{F} is defined as

$$(5.7) \quad \bar{F}(h, v; B) := \max_{t \in [0, T_F]} f^{ob}(h, v; B, t) = \max_{t \in [0, T_F]} \int_c^d [h(x, t) + B_0(x)] dx.$$

In the definition of F , we consider the variables h and v functions of B through the solution of the shallow water equations. Thus, the probability we aim at estimating is the probability that the maximum average wave height in $[c, d]$ exceed a threshold z , where B follows the distribution introduced in subsection 5.2.

The function \bar{F} (5.7) involves the max-function, which makes optimization difficult. Thus, for $\gamma > 0$ we introduce the regularized parameter-to-event map $F_\gamma : B \mapsto \bar{F}_\gamma(h(B), v(B); B)$, where

$$(5.8) \quad \bar{F}_\gamma(h, v; B) := \gamma \log \left[\frac{1}{T_F} \int_0^{T_F} \exp \left(\frac{1}{\gamma} \int_c^d (h + B_0) dx \right) dt \right].$$

The smaller γ , the better (5.8) approximates (5.7). In particular,
(5.9)

$$\lim_{\gamma \rightarrow 0} \bar{F}_\gamma(h, v; B) = \lim_{\gamma \rightarrow 0} \gamma \log \left[\frac{1}{T_F} \int_0^{T_F} \exp \left(\frac{f^{ob}(h, v; B, T)}{\gamma} \right) dt \right] = \max_{t \in [0, T_F]} f^{ob}(h, v; B, T).$$

5.4. LDT-optimization. Given the parameter space, the governing equations and the event measure, we now detail the LDT optimization problem (2.20) over the parameter $B \in \mathcal{B}$. For the tsunami problem, $I(B)$ and $F(B)$ are defined in (5.5) and (5.7) (or (5.8)), respectively. The parameter-to-event map F involves the PDE (5.2) with zero initial conditions and proper boundary conditions, which we omit in the following discussions for brevity. Since we consider the two parameter-to-event maps (5.7) and (5.8), we obtain two LDT optimization problems.

Regularized objective. Using the regularization parameter-to-event map (5.8), the LDT problem is the PDE-constrained optimization problem

$$(5.10) \quad \min_{B, h, v} I(B) - \lambda \bar{F}_\gamma(h, v; B),$$

subject to the PDE constraints (5.2).

For subsequent use, we define the reduced objective $J_{\gamma, \lambda}(B) := I(B) - \lambda F_\gamma(B)$. Thus, the PDE-constrained problem (5.10) can be written as unconstrained optimization problem over $B \in \mathcal{B}$. While the objective $J_{\gamma, \lambda}(\cdot)$ is smooth, its accurate evaluation can become difficult for small $\gamma > 0$, and its gradients can be large. An alternative to this regularized objective is to consider the time of the largest average wave height close to shore as an additional unknown, resulting in the second problem.

Time-optimal problem. We can also consider a time-optimal LDT optimization that does not require a regularization parameter γ . Using the definition of \bar{F} in (5.7), additional optimization over the time results in the PDE-constrained optimization problem

$$(5.11) \quad \min_{\substack{B, h, v, \\ t \in [0, T_F]}} I(B) - \lambda f^{ob}(h, v; B, t),$$

subject to the PDE constraints (5.2).

The corresponding reduced objective is $J_\lambda(B, t) := I(B) - \lambda f^{ob}(h(B), v(B); B, t)$, where $h(B)$ and $v(B)$ are again the solutions of shallow water equations (5.2).

5.5. Discretization and stabilization. To solve the optimization problems (5.10) and (5.11) numerically, we have to discretize the continuous functions B , v , h together with the governing equations. Since the shallow water equations (5.12) are hyperbolic, we use a discontinuous Galerkin finite element method (DG-FEM) [29] to discretize the equations in space. For discretization in time, we use a Runge-Kutta scheme.

Since the shallow water equations (5.2) are a system of nonlinear hyperbolic equations, the solution can have shocks, i.e., the slope of the solution variables can become infinite. It is well known that the numerical approximation of systems with shocks is challenging [34]. This is even more compounded for adjoint-based derivative computation. Some of the discretization and stabilization choices we make here are in fact motivated by our focus on adjoint-based derivatives, as will become clear in the subsequent

subsections. Partially motivated by the need for well-defined discrete adjoint equations (see [subsection 5.7](#)), we add artificial viscosity to the shallow water equations (5.2) to prevent slopes that cannot be resolved by the discretization. There are different approaches of adding artificial viscosity to the shallow water equations. One is adding viscosity for both the mass and momentum conservation laws [10]. Here, we only add viscosity to the momentum equation, as discussed in [38], where the authors prove that the solutions of the resulting system preserves stationary steady states and is asymptotically stable. This modified problem is

$$(5.12a) \quad h_t + v_x = 0 \quad \text{on } \mathcal{D} \times [0, T_F],$$

$$(5.12b) \quad v_t + \left(\frac{v^2}{h} + \frac{1}{2}gh^2 - \epsilon h\varphi \right)_x + ghB_x = 0 \quad \text{on } \mathcal{D} \times [0, T_F],$$

$$(5.12c) \quad \varphi + \left(-\frac{v}{h} \right)_x = 0 \quad \text{on } \mathcal{D} \times [0, T_F],$$

with the initial and boundary conditions (5.2c) and (5.2d). Here, $\varphi(x, t)$ serves as an auxiliary variable which allows to write the dissipative operator in a way suitable for a DG scheme. The parameter ϵ controls how much artificial viscosity is added, and we choose $\epsilon = O(|\bar{h}|)$ with \bar{h} being the element length as proposed in [34, 48].

Our implementation uses a DG discretization with linear interpolating polynomials in space. For (5.12a) and (5.12b), we use a global Lax-Friedrichs flux of the form

$$(5.13) \quad f^*(q) = \frac{f(q^-) + f(q^+)}{2} + \frac{C^{LF}}{2} n^- (q^- - q^+),$$

where q stands for either h or v . Moreover, $f(q)$ is the corresponding flux, $+$ and $-$ denote the exterior and the interior value at each element interface, and C^{LF} is the global Lax-Friedrichs constant. A less diffusive alternative to a global Lax-Friedrichs flux would be a local variant, where the flux at each interface depends on the state variable. While using such a local flux in the context of adjoint equations might be possible, here we prefer to avoid technical challenges and possible inconsistencies and use the same global Lax-Friedrichs constant C^{LF} for all elements:

$$(5.14) \quad C^{LF} = \max\left(\left|\frac{v}{h}\right| + \sqrt{gh}\right).$$

For (5.12c), we use a central flux in the DG scheme, i.e., the average of the values at the interfaces. Although the numerical results presented in this paper use a first-order DG scheme, the proposed method can be generalized to higher-order spatial discretizations. To discretize in time, we use a strong stability-preserving second-order Runge-Kutta (SSP-RK2) method [29]. The strong stability-preserving (SSP) property guarantees preservation of the total variation of the discrete solution.

5.6. Adjoint-based gradient computation. Since the objectives $J_\lambda(\cdot)$ and $J_{\gamma,\lambda}(\cdot)$ require the solution of a PDE, we use adjoints to efficiently compute their derivatives [5, 12, 30, 47]. Here, we present the continuous form of these adjoint equations. Their discretization is summarized in [subsection 5.7](#). We skip details of the technical derivation and only present the results, starting with the regularized objective.

Regularized objective. To derive the adjoint system for the shallow water equations with artificial viscosity (5.12), we use a formal Lagrangian approach, i.e., we define the Lagrangian as the sum of the objective and the weak form of the state equations, where the test functions take the role of the Lagrange multiplier functions. Then, setting variations with respect to the state variables in all directions to zero results in the adjoint equations in the unknowns (p, w, ψ) :

$$(5.15a) \quad p_t + \left(-\frac{v^2}{h^2} + gh - \epsilon\varphi \right) w_x - \frac{v}{h^2} \psi_x - gB_x w + \lambda \partial_h \bar{F}_\gamma = 0 \quad \text{on } \mathcal{D} \times [0, T_F],$$

$$(5.15b) \quad w_t + p_x + \frac{2v}{h} w_x - \frac{1}{h} \psi_x = 0 \quad \text{on } \mathcal{D} \times [0, T_F],$$

$$(5.15c) \quad \psi - \epsilon h w_x = 0 \quad \text{on } \mathcal{D} \times [0, T_F],$$

$$(5.15d) \quad p(x, T_F) = 0, \quad w(x, T_F) = 0 \quad \text{for } x \in \mathcal{D},$$

$$(5.15e) \quad w(a, t) = w(b, t) = 0 \quad \text{for } t \in [0, T_F].$$

Here, the partial derivative of \bar{F}_γ with respect to h is defined as

$$\partial_h \bar{F}_\gamma := \frac{1}{T_F} \exp \left\{ \frac{1}{\gamma} \left[\int_c^d (h + B_0) dx - \bar{F}_\gamma \right] \right\}, \quad \text{on } [c, d] \times [0, T_F],$$

and $\partial_h \bar{F}_\gamma := 0$ else. When solving the adjoint system (5.15), the state variables (v, h, φ) are known and we only solve for the adjoint variables (p, w, ψ) , which appear linear in (5.15). Note that due to (5.15d), this is a final value problem that must be solved backwards in time. Once the state and the adjoint variables are known, one can obtain the derivative $\mathcal{G}(B)(\hat{B})$ of $J_{\gamma, \lambda}$ in an arbitrary direction $\hat{B} = O\hat{S}$ as the variation of the Lagrangian with respect to $B = B_0 + OS$ in that direction, i.e.

$$(5.16) \quad \mathcal{G}(B)(\hat{B}) = \langle B - B_0, \hat{B} \rangle_{C_s} + \int_0^{T_F} \int_{\mathcal{D}} ghw \hat{B}_x dx dt = S^\top C_s^{-1} \hat{S} + \int_0^{T_F} \int_{\mathcal{D}} ghw (O\hat{S})_x dx dt.$$

Time-optimal objective. For the time-optimal problem (5.11), additionally to the derivative with respect to B , we require derivatives with respect to the observation time t . Again, we skip details here—optimization over time or time-optimal control is a challenging research topic by itself [21, 32].

The main difference between J_λ and $J_{\gamma, \lambda}$ is that in the latter, $\bar{F}_\gamma(h, v; B)$ is replaced by $f^{ob}(h, v; B, t)$. Thus, one obtains the adjoint equations for the time optimal problem (5.11) by replacing $\partial_h \bar{F}_\gamma$ in (5.15) with the derivative of f^{ob} with respect to h , i.e., $\partial_h f^{ob} := 1/|d - c|$ on $[c, d] \times [0, T_F]$ and $\partial_h f^{ob} := 0$ else. Additionally, the final time conditions becomes $p(x, T_F) = \lambda/|d - c|$ for $x \in [c, d]$ and $p(x, T_F) = 0$ else. Since F_γ and f^{ob} do not depend explicitly on B , the gradient of J_λ is identical to (5.16).

Finally, we require the derivative of J_λ with respect to the observation time t . A short computation yields that

$$(5.17) \quad \frac{\partial}{\partial t} J_\lambda(B, t) = -\lambda \frac{\partial}{\partial t} f^{ob}(h, v; B, t) = -\lambda \int_c^d \frac{\partial}{\partial t} h(x, t) dx = \lambda \int_c^d \frac{\partial}{\partial x} v(x, t) dx,$$

where the last identity follows from the conservation-of-mass equation $h_t + v_x = 0$.

5.7. Discretization of adjoint equations and gradient. When shocks occur in the state equations, this may lead to discontinuous coefficients in the adjoint equations. Thus, the theory and grid convergence of adjoint-based gradients for hyperbolic systems is challenging and rigorous results are rare. The authors of [24] study the grid convergence of the adjoint solutions for Burger’s equation, and find that solutions of the finite difference-discretized equation may converge to a wrong continuous solution when the state solution has shocks. To smooth out shocks that cannot be resolved by the mesh, they propose adding artificial viscosity that vanishes at a certain rate as the mesh is refined. The result on the required rate has been improved recently [48]. As discussed in subsection 5.5, we follow a similar strategy in the context of a discontinuous Galerkin discretization for the shallow water equations.

To discretize the adjoint equations and the gradient expressions from the previous section, we follow a discretize-then-optimize approach, i.e., we first discretize the optimization objective and the governing equations in space and time, and then compute discrete derivatives. This means that the discretization of the adjoint equation is implied by that of the state equation. An alternative would be the optimize-then-discretize approach, which discretizes the continuous adjoint equation independently. While more convenient, this may result in inconsistent gradients, i.e., numerically gradients that are not exact gradients of any discrete (or continuous) problem. Both approaches have their advantages and disadvantages, but here we follow the former approach, i.e., discretize the problem and then compute the corresponding adjoint-based gradient. In the previous section we nevertheless presented the continuous adjoint equations to show and discuss their structure. We suppress the (interesting) technical details of the following computations for space reasons, and only summarize the results.

Following this discretize-then-optimize approach, we find that the adjoint of the spatial DG-discretization of (5.12) is again a DG discretization of the continuous adjoint equations, extending results in [53] to nonlinear conservation laws. The induced flux in the adjoint equations is a modified global Lax-Friedrichs flux. We follow the same discretize-then-optimize approach for the Runge-Kutta time discretization. Results in [27] show that the SSP property for the state equation ensures stability of the discrete adjoint time-stepping scheme. While the adjoint time-adjoint method does not coincide with the SSP-RK2 scheme, it is also a second-order scheme that preserves stability. Since the regularized objective \bar{F}_γ involves integration over time and we use the quadrature induced by SSP-RK2 for its discretization. The bathymetry B is discretized using linear continuous finite elements. The embedding of linear continuous to discontinuous elements as needed in (5.12) is trivial, and the adjoint of this embedding is used to transfer the gradient from the discontinuous to the continuous space.

Due to the use of a DG scheme and the discretize-then-optimize approach, the gradient expressions include additional terms at element interfaces, as observed for linear problems [53]. These additional terms vanish in the limit as the mesh is refined, but they must be included to obtain exact gradients of the discretized problem. To avoid the technical derivations, we only present the continuous forms of the gradient in (5.16). We verify the correctness of our gradient implementation, by comparing directional derivatives with their finite differences approximations. Due to the discretize-then-optimize approach, they coincide not only for physics-resolving, but also for coarse meshes up to

Table 1

Number of iterations for different λ 's, for optimization with regularized objective F_γ in (5.10) with $\gamma = 0.003$, and with time-optimal objective (5.11). The iteration is terminated when the C^{-1} -weighted norm of the gradient is reduced by 5 orders of magnitude. Shown are also the values of $z = z(\lambda)$ and the event probability estimate computed using a second-order approximation of $\Omega(z)$.

| λ | Regularized objective F_γ | | | Time-optimal problem | | |
|-----------|----------------------------------|-------------|--------|------------------------|-------------|--------|
| | $z := F_\gamma(B^*(\lambda))$ | $P^{SO}(z)$ | # iter | $z := F(B^*(\lambda))$ | $P^{SO}(z)$ | # iter |
| 12 | 0.263 | 4.80e-02 | 23 | 0.281 | 4.70e-02 | 35 |
| 16 | 0.364 | 9.55e-03 | 31 | 0.382 | 9.36e-03 | 27 |
| 20 | 0.468 | 1.24e-03 | 24 | 0.486 | 1.22e-03 | 20 |
| 24 | 0.574 | 1.04e-04 | 31 | 0.592 | 1.02e-04 | 20 |
| 28 | 0.682 | 5.45e-06 | 27 | 0.701 | 5.33e-06 | 30 |
| 32 | 0.792 | 1.77e-07 | 33 | 0.811 | 1.73e-07 | 27 |
| 36 | 0.905 | 3.54e-09 | 29 | 0.923 | 3.45e-09 | 34 |
| 40 | 1.018 | 4.27e-11 | 32 | 1.037 | 4.17e-11 | 38 |
| 44 | 1.134 | 3.09e-13 | 30 | 1.152 | 3.02e-13 | 30 |
| 48 | 1.250 | 1.36e-15 | 37 | 1.269 | 1.26e-15 | 35 |

what can be expected in the presence of machine round-off.

6. Results for tsunami problem. Here, we study the convergence behavior of the proposed algorithms and approximations. We also discuss qualitative results such as the bathymetry change resulting in the most extreme tsunami event and extreme event probabilities. First, we discuss the numerical solution of the LDT optimization problems.

6.1. Shallow water equation-constrained optimization. To compute minimizers for (2.20), we need to solve the PDE-constrained optimization problems (5.10) and (5.11). We use the adjoint method discussed in subsection 5.6 to compute gradients and use a preconditioned steepest descent method for the optimization. Backtracking line search using the Armijo rule [39] is used for globalization of the descent algorithm. We precondition the gradient with the covariance matrix.

In Table 1, we present iterations numbers for different values of λ , as well as the corresponding extreme event values and probability estimates based on the second-order approximation discussed in subsection 4.1. For each λ , we take the reference bathymetry B_0 as the starting point for the optimization. We observe in Table 1 that the iteration numbers are generally insensitive to λ for both the regularized and the time-optimal problem. Since larger λ 's correspond to extremier events, we find in particular that the number of iterations is independent of the extremeness of events. This is a desirable property that often does not hold for sampling-based methods.

Figure 6 shows the optimal bathymetry changes $B^* - B_0$ for different values of λ , and thus different extreme event thresholds z . We show results for the regularized and the time-optimal formulations (5.10) and (5.11). Since γ is chosen rather small, there is visually little difference between the optimizers found with these different formulations. As can be seen, the most effective mechanism for large tsunamis on shore involves an uplift in the shore-facing part and a downlift away from the shore. The corresponding slips generating these bathymetry changes can be seen on the right in Figure 6. The 20 slip patches all move in the same direction and the slip is larger in the middle than at the sides of the slip area. Since tsunami waves interact with the bathymetry, these

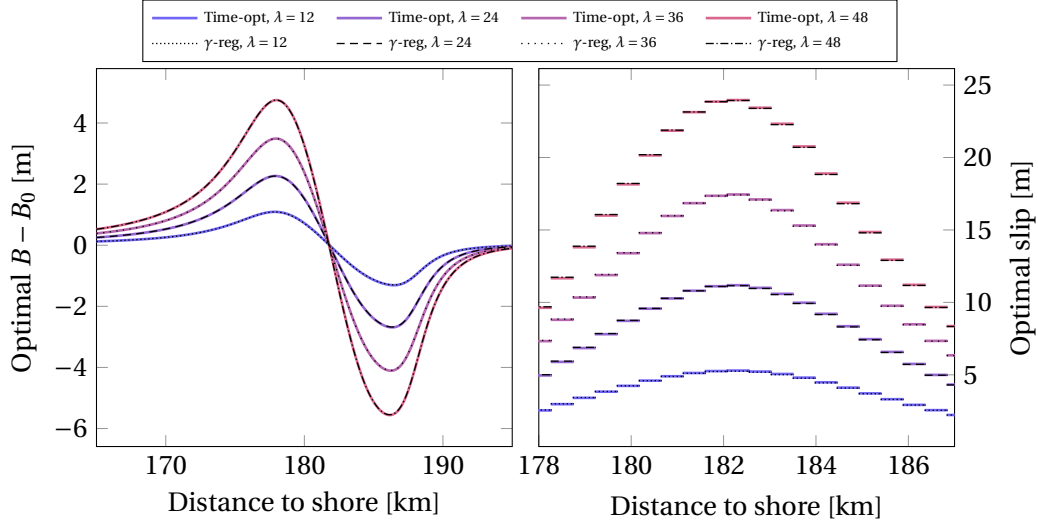


Figure 6. Shown on the left are optimal bathymetry changes of LDT-solutions B^* for different λ 's (time optimal and regularized objective F_γ with $\gamma = 0.003$). For fixed λ , the optimizers of the two problems are quite similar, showing that the approximation of the max-function with F_γ is quite effective. Shown on the right are fault slips corresponding to the optimal solutions B^* for different λ 's as discussed in subsection 5.2.

optimal patterns depend, at least to some degree, on the structure of the bathymetry and the location where the event is observed.

Note that optimizers for different λ have a similar structure but their magnitude varies with the extremeness of the event. To explain these magnitude differences, recall that the rate function I is quadratic. If the parameter-to-event map F were linear, then the LDT minimizer would increase linearly with λ as can be seen from the optimality conditions of such a quadratic optimization objective. Deviations from that scaling are a result of the nonlinearity in the parameter-to-event map caused by the nonlinearity of the shallow water equation and the extreme event objective. Since this deviation is small, we deduce that the problem is moderate nonlinear. This (together with the results presented in the subsequent subsection 6.3) indicates a posteriori that the assumptions needed for our LDT theory are likely satisfied in this problem.

6.2. Eigenvalue estimation for second-order approximation $P^{SO}(z)$. As discussed in subsection 4.1, computing the prefactor using (4.13) requires estimation of the eigenvalues of the Hessian of the parameter-to-observable map, preconditioned with the covariance of the Gaussian parameter distribution, i.e., $(OC_s^{1/2})^\top \nabla_B^2 F(B^*) OC_s^{1/2}$. Here, we study the feasibility of this approach for the tsunami problem. In these numerical tests we approximate the Hessian-application using finite differences of gradients.

As discussed in subsection 5.2, the random parameter B is modeled using 20 slips at the fault boundary below the ocean floor. Thus, and due to typical properties of covariance matrices, we argued in subsection 4.2 that the eigenvalues of this preconditioned Hessian decay rapidly. To verify this numerically, we compute the eigenvalues of preconditioned Hessians for different λ 's and multiply them by λ as in Theorem 4.2. The results for the tsunami problem are shown in Figure 7. It can be seen that the eigenvalues decay

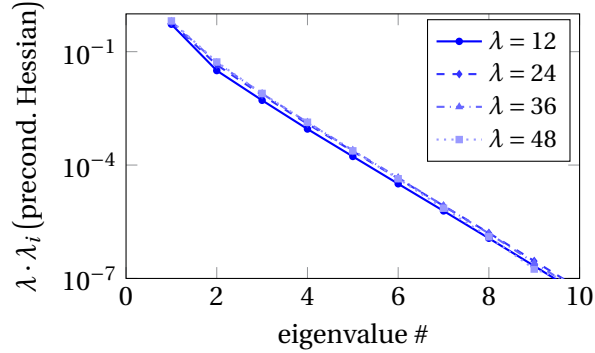


Figure 7. Shown are the dominating eigenvalues of the preconditioned Hessian multiplied with the corresponding λ defined in [Theorem 4.2](#) for various values of λ . The eigenvalues that are small compared to 1 have little influence on $P^{SO}(z)$, i.e., computation of about 5 eigenvalues is sufficient in our example. Note that the rapid decay is insensitive to λ , and thus to how extreme the event is.

rapidly and this behavior barely changes with the extremeness of the event. This shows that it is sufficient to use a small number of dominating eigenvalues in the second-order approximation. However, the largest value of about 0.5 indicates non-negligible non-linearity of the parameter-to-event map F . If F were linear, all eigenvalues would be zero. In addition, we find that all leading eigenvalues are positive, indicating that F is convex in all leading directions close to the LDT-minimizers. This results in a larger-than-one multiplicative SORM-correction term [\(4.14\)](#). Thus, the probability estimate from the first-order approximation is smaller than the estimate from the second-order approximation.

6.3. Comparison of extreme event quantification methods. In this section, we compare the proposed extreme event estimation methods for the Tohoku-Oki tsunami. In the [Figures 8](#) and [9](#), we compare the results of Monte Carlo sampling with the LDT approaches (constant prefactor estimated by fitting with MC data, the first and second-order approximation of the set $\Omega(z)$) for both the regularized objective problem [\(5.10\)](#) and the time optimal problem [\(5.11\)](#). The reference probability for moderately extreme events is computed with Monte Carlo sampling with 10^5 samples using the estimator $P_N^{MC}(z)$ in [\(3.1\)](#). This procedure is clearly very costly in particular when one is interested in extreme events. We also show the 95% confidence interval for the estimator, which is tight for $z < 0.4$. However, the Monte Carlo estimator $P_N^{MC}(z)$ only provides acceptable accuracy for a probability down to about 10^{-4} . We also use the LDT logarithmic rate with a constant prefactor as discussed in [subsection 3.2](#), fitting the Monte Carlo results in the interval $z \in [0.2, 0.4]$. The resulting estimate seems to overestimate the extreme event probability. It also requires MC sampling for estimating the fitting constant. The first and second-order approximation of $\Omega(z)$ do not require fitting since they rely only on the LDT-optimizers and the local derivative information around the optimizers. The first-order approximation results in [Figures 8](#) and [9](#) are below the Monte Carlo estimator, showing that significant parts of $\Omega(z)$ are not contained in the half-space $\mathcal{H}(z)$. The second-order approximation results in [Figures 8](#) and [9](#) are closer to the MC estimator, indicating that the second-order approximation of $\Omega(z)$ describes the set $\Omega(z)$ well. All

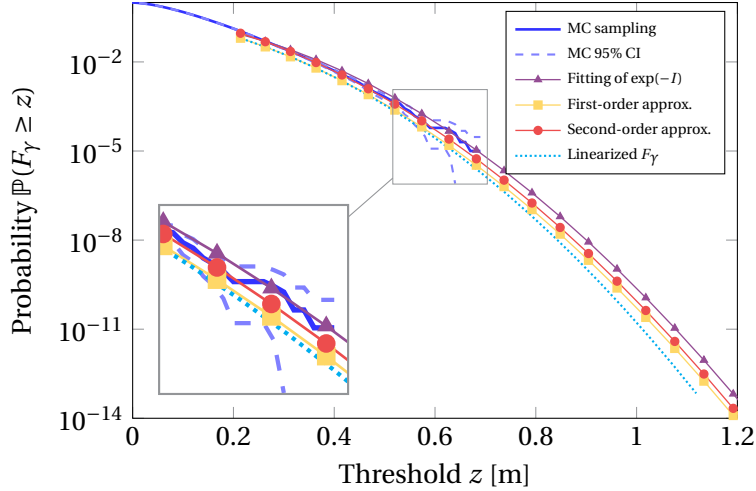


Figure 8. Comparison of probability estimation for regularized objective F_γ (5.8) with $\gamma = 0.003$. Shown in blue are the mean and 95% confidence intervals obtained with standard MC with 10^5 samples (discussed in subsection 3.1), in purple results obtained by fitting the asymptotic LDT rate with the MC mean (subsection 3.2), and results using first-order and second-order approximation of $\Omega(z)$ (Appendix B and subsection 4.1) in red and yellow, respectively. Each marker represents the solution of an LDT optimization problem with a different value of λ . The zoom-in shows the regime where the variance of the standard MC sampling method increases and standard MC sampling becomes infeasible. For comparison, the cyan dotted line shows the probabilities obtained by linearization of F_γ at the optimizer B^* for $\lambda = 12$.

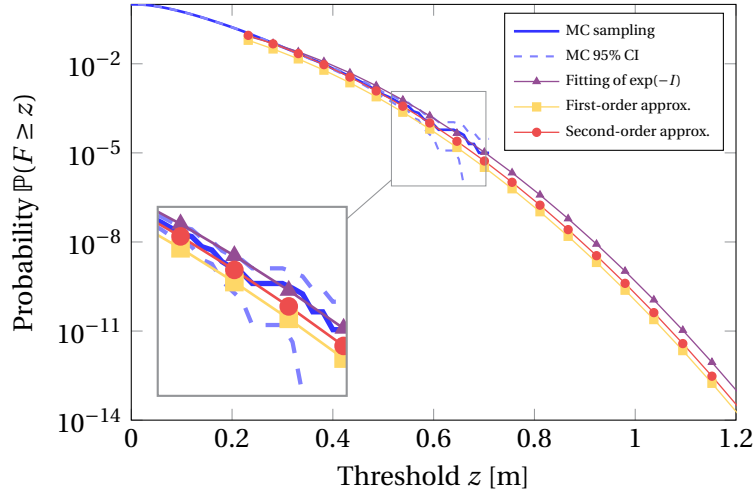


Figure 9. Same as Figure 8, but for time-optimal objective F defined in (5.7).

approaches provide probability estimates down to 10^{-14} . Comparing the results in Figures 8 and 9 shows that there is little difference between the time-optimal formulation and the regularization formulation with $\gamma = 0.003$. In Figure 8, we additionally show the extreme event probabilities computed using a linear parameter-to-event map, namely F_γ linearized around B^* , the LDT-optimizer for $\lambda = 12$. When the parameter-to-event map is linear, the extreme event set is a half-space over which we can integrate the rate

function exactly. The resulting values shown in Figure 8 underestimate the extreme event probability and results in an incorrect asymptotic rate. This highlights the role of the nonlinearity in the parameter-to-event map.

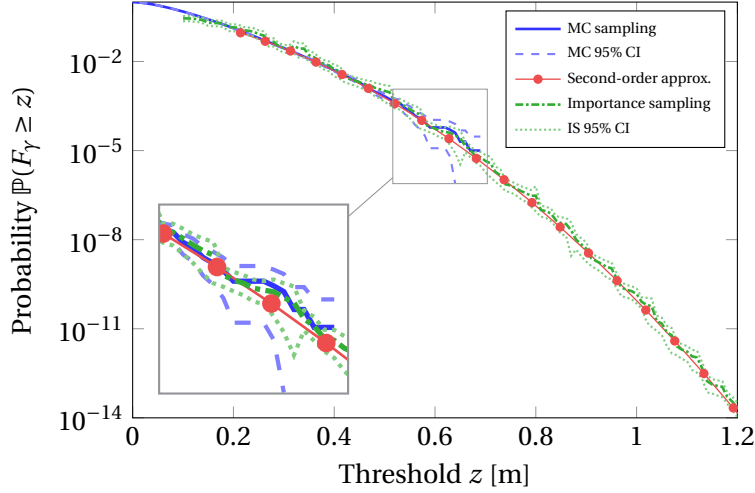


Figure 10. Comparison of estimation using IS for regularized objective F_γ with $\gamma = 0.003$. In green we show the mean and 95% confidence intervals obtained with IS. The results obtained with standard MC sampling and second-order approximation of $\Omega(z)$ are as in Figure 8 and shown for comparison. For IS, the same LDT minimizers for different values of λ as for the second-order approximation are used. We use 100 samples for each LDT-optimizer to estimate the probability following (3.7). For other values of z , we use the samples at the nearest minimizer to estimate the probability. As can be seen, the IS results align well with the results from the second-order approximation.

The results obtained with IS are shown in Figure 10. For each λ also used in Figure 8, we use 100 samples from the shifted distribution centered at the optimizer B^* to compute (3.8) at $z = z(\lambda)$, and in a neighborhood. Note that IS based on the shift of the mean is efficient even for large z , which correspond to extreme events. Despite only using 100 samples, we obtain tight 95% confidence intervals. We only show the results for the regularized objective F_γ , but IS applies analogously to F using the time-optimal optimizers, and we have obtained similar results. In particular, IS with 100 samples has comparable accuracy as SORM in Figure 9.

To make the comparison between the different methods easier, we compare results obtained with different methods for estimating the prefactor $C_0(z)$ in Figure 11. As can be seen, the second-order approximation of $C_0(z)$ converges to the prefactor estimated using IS as z increases, which demonstrates that the second-order approximation (4.13) is an asymptotic estimation of the original probability $P(z)$ as discussed in subsection 4.1. In contrast, the first-order estimation of $C_0(z)$ does not converge to the IS estimated prefactor, demonstrating that the correction factor computed by the second-order approximation is crucial. These observations are consistent with our discussion in subsection 4.1 and Appendix B.

7. Discussions and conclusions. In this paper, we use arguments from LDT to relate probability estimation of extreme events to optimization problems. These optimization problems typically involve solving a PDE, and thus we apply the adjoint method

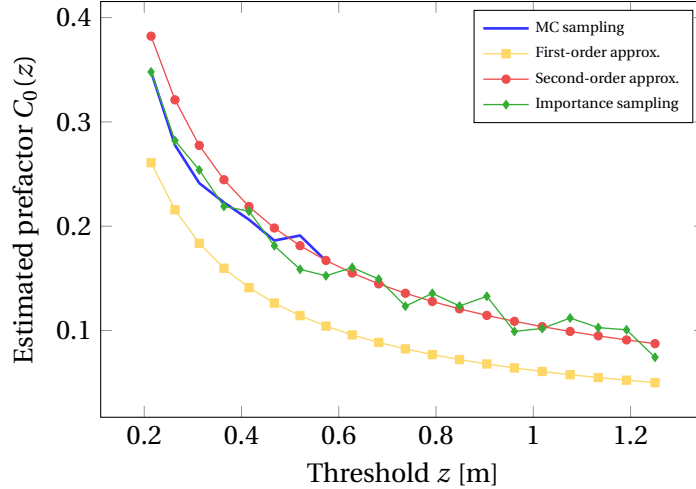


Figure 11. Comparison of estimated prefactor for regularized objective F_γ (5.8) with $\gamma = 0.003$ as also uses in Figures 8 and 10. Shown is the estimated prefactor $C_0(z) = \mathbb{P}(F_\gamma \geq z) / \exp(-I(\theta^*(z)))$ with 10^5 samples of vanilla MC (blue), and estimations using an first-order and second-order approximation of $\Omega(z)$ (Appendix B and subsection 4.1) in red and yellow, respectively. Each marker represents the solution of an LDT optimization problem with a different value of λ . The green line shows the IS estimation of C_0 . Since only 10^3 samples are used for each optimizer, sampling error is still visible.

to compute derivatives efficiently in a manner that is independent of the parameter space dimension. Additionally, we observe numerically that the number of iterations required to solve these LDT optimization problems is insensitive to the extremeness of the event. If the underlying parameter distribution is a multivariate Gaussian distribution, the LDT-prefactor required for the probability estimate can be computed using either (1) a second-order approximations of the extreme event set boundary combined with a randomized SVD or (2) importance sampling with a proposal centered at the LDT optimizer. We observe that the cost of these methods is either independent or depends only weakly on how extreme the event is. Moreover, it is independent of the discretization dimensions. This is a significant improvement over MC methods whose performance typically suffers from the parameter dimension and the level of extremeness of the event. Since the method based on the second-order set approximation appears to be accurate and does not require MC sampling, it might be a good candidate for applications where the target is the control or mitigation of extreme events.

Our main application is a 1D tsunami problem, which is a simplification from realistic two-dimensional tsunamis. It is definitely interesting to expand this application to 2D. The main methods including the optimization formulation from LDT and the approximation using first/second-order information will remain as in 1D. The main challenges are technical, i.e., modeling tsunami waves and a realistic bathymetry in 2D, and deriving and implementing the corresponding adjoint equations.

Appendix A. Examples of rate functions $I(\theta)$ for different distributions $\mu(\theta)$. Here, we provide examples of the derivation of rate functions for different distributions.

Example A.1 (Multivariate normal distribution in \mathbb{R}^n). Consider a multivariate ran-

dom variable $\theta \sim \mathcal{N}(\theta_0, C)$. The cumulant generating function $S(\eta)$ is

$$\begin{aligned}
 S(\eta) &= \log \int_{\Omega} e^{\langle \eta, \theta \rangle} (2\pi)^{-\frac{n}{2}} (\det C)^{-\frac{1}{2}} e^{-\frac{1}{2}(\theta - \theta_0)^\top C^{-1}(\theta - \theta_0)} d\theta \\
 (A.1) \quad &= \log \left[e^{\eta^\top \theta_0 + \frac{1}{2} \eta^\top C \eta} \cdot \int_{\Omega} (2\pi)^{-\frac{n}{2}} (\det C)^{-\frac{1}{2}} e^{-\frac{1}{2}(\theta - \theta_0 - C\eta)^\top C^{-1}(\theta - \theta_0 - C\eta)} d\theta \right] \\
 &= \log \left[e^{\eta^\top \theta_0 + \frac{1}{2} \eta^\top C \eta} \cdot 1 \right] = \eta^\top \theta_0 + \frac{1}{2} \eta^\top C \eta.
 \end{aligned}$$

Thus, the rate function $I(\theta)$ for a multivariate Gaussian distribution is

$$\begin{aligned}
 (A.2) \quad I(\theta) &= \max_{\eta \in \mathbb{R}^n} \left(\eta^\top \theta - \eta^\top \theta_0 - \frac{1}{2} \eta^\top C \eta \right) \\
 &= [C^{-1}(\theta - \theta_0)]^\top (\theta - \theta_0) - \frac{1}{2} [C^{-1}(\theta - \theta_0)]^\top C [C^{-1}(\theta - \theta_0)] = \frac{1}{2} \|\theta - \theta_0\|_{C^{-1}}^2,
 \end{aligned}$$

since the maximum is obtained at $\eta = C^{-1}(\theta - \theta_0)$. Thus, $I(\theta)$ is, up to a normalization constant, the negative log-probability density of θ . Hence, for a Gaussian distribution, the LDT optimization problem (1.2) is finding the most probable point, i.e., the point maximizing the log-density.

While in this paper we focus on finite dimensional random variables, we show that the previous example generalizes to Gaussian random fields.

Example A.2 (Gaussian random field). Assume that the parameter is a Gaussian random field $\theta(x) \sim \mathcal{N}(\theta_0(x), \mathcal{C})$. Here, \mathcal{C} is a trace-class covariance operator defined over a Hilbert space Ω . For instance, $\Omega = L^2(\mathcal{D})$ for a physical domain $\mathcal{D} \subset \mathbb{R}^n$, $n \in \{1, 2, 3\}$, and thus each sample θ is a real-valued function over \mathcal{D} . An example for such a covariance operator is $\mathcal{C} = (-\Delta + \gamma I)^{-2}$, $\gamma > 0$, with appropriate boundary conditions. The parameter $\theta(x)$ has the Karhunen-Loève expansion $\theta(x) = \theta_0(x) + \sum_{j=1}^{\infty} \sqrt{\lambda_j} \xi_j e_j(x)$, $x \in \mathcal{D}$, where ξ_j are independent standard normal variables $\xi_j \sim \mathcal{N}(0, 1)$, and $\lambda_j > 0$, e_j are eigenvalues and orthonormal eigenfunctions of \mathcal{C} , i.e., $\mathcal{C} e_j = \lambda_j e_j$ [33]. Let $\eta \in \Omega$, then $\langle \eta, \theta \rangle = \langle \eta, \theta_0 \rangle + \sum_{j=1}^{\infty} \sqrt{\lambda_j} \xi_j \langle \eta, e_j \rangle$. For the cumulant generating function $S(\eta)$, we obtain

$$\begin{aligned}
 S(\eta) &= \log \int_{\Omega} e^{\langle \eta, \theta_0 \rangle + \sum_{j=1}^{\infty} \sqrt{\lambda_j} \xi_j \langle \eta, e_j \rangle} d\mu(\theta) = \log \left(e^{\langle \eta, \theta_0 \rangle} \prod_{j=1}^{\infty} \int_{\mathbb{R}} e^{\sqrt{\lambda_j} \xi_j \langle \eta, e_j \rangle} e^{-\frac{1}{2} \xi_j^2} d\xi_j \right) \\
 &= \langle \eta, \theta_0 \rangle + \sum_{j=1}^{\infty} \log \int_{\mathbb{R}} e^{\sqrt{\lambda_j} \xi_j \langle \eta, e_j \rangle} \frac{1}{\sqrt{2\pi}} e^{-\frac{1}{2} \xi_j^2} d\xi_j \\
 &= \langle \eta, \theta_0 \rangle + \sum_{j=1}^{\infty} \log \left(e^{\frac{1}{2} \lambda_j \langle \eta, e_j \rangle^2} \int_{\mathbb{R}} \frac{1}{\sqrt{2\pi}} e^{-\frac{1}{2} (\xi_j - \sqrt{\lambda_j} \xi_j \langle \eta, e_j \rangle)^2} d\xi_j \right) = \langle \eta, \theta_0 \rangle + \sum_{j=1}^{\infty} \frac{1}{2} \lambda_j \langle \eta, e_j \rangle^2.
 \end{aligned}$$

The corresponding rate function $I(\theta)$ is

$$I(\theta) = \max_{\eta \in \Omega} \left[\langle \eta, \theta \rangle - \left(\langle \eta, \theta_0 \rangle + \sum_{j=1}^{\infty} \frac{1}{2} \lambda_j \langle \eta, e_j \rangle^2 \right) \right]$$

For any given θ , the optimal η for the above maximization problem should satisfy the first-order optimality condition, i.e., $\theta - \theta_0 - \sum_{j=1}^{\infty} \lambda_j \langle \eta, e_j \rangle e_j = 0$. Thus, the maximum is

obtained for $\eta = \sum_{j=1}^{\infty} \lambda_j^{-1} \langle \theta - \theta_0, e_j \rangle e_j$. Plugging in this η and using the facts that $\theta - \theta_0 = \sum_{j=1}^{\infty} \langle \theta - \theta_0, e_j \rangle e_j$ and $\{e_j\}$ is an eigenfunction basis of \mathcal{C} , we obtain:

$$\begin{aligned} I(\theta) &= \left\langle \sum_{i=1}^{\infty} \frac{1}{\lambda_i} \langle \theta - \theta_0, e_i \rangle e_i, \theta \right\rangle - \left(\left\langle \sum_{i=1}^{\infty} \frac{1}{\lambda_i} \langle \theta - \theta_0, e_i \rangle e_i, \theta_0 \right\rangle + \sum_{j=1}^{\infty} \frac{1}{2} \lambda_j \left\langle \sum_{i=1}^{\infty} \frac{1}{\lambda_i} \langle \theta - \theta_0, e_i \rangle e_i, e_j \right\rangle^2 \right) \\ &= \frac{1}{2} \sum_{j=1}^{\infty} \frac{1}{\lambda_j} \langle \theta - \theta_0, e_j \rangle^2 = \frac{1}{2} \|\theta - \theta_0\|_{\mathcal{C}^{-1}}^2. \end{aligned}$$

The above computations only hold for θ such that all infinite sums converge. Otherwise, we define $I(\theta) := \infty$.

Example A.3 (Exponential distribution). Consider a parameter θ with n independent components θ_k 's, each of which satisfies an exponential distribution with $\alpha_k > 0$, i.e.,

$$(A.3) \quad d\mu(\theta) = \prod_{k=1}^n \alpha_k e^{-\alpha_k \theta_k} d\theta_k \quad \text{for } \theta_k \geq 0.$$

The corresponding cumulant generating function $S(\eta)$ is

$$(A.4) \quad S(\eta) = \log \prod_{k=1}^n \int_0^{\infty} e^{\eta_k \theta_k} \alpha_k e^{-\alpha_k \theta_k} d\theta_k = - \sum_{k=1}^n \log \left(1 - \frac{\eta_k}{\alpha_k} \right) \quad \text{for } \eta_k < \alpha_k.$$

The associated rate function is

$$(A.5) \quad I(\theta) = \max_{\eta \in \mathbb{R}^n, \eta_k < \alpha_k} \left[\langle \eta, \theta \rangle + \sum_{k=1}^n \log \left(1 - \frac{\eta_k}{\alpha_k} \right) \right] = \sum_{k=1}^n (\alpha_k \theta_k - 1 - \log \theta_k) \quad \text{for } \theta_k > 0,$$

since the maximum is reached for $\eta_k = \alpha_k - 1/\theta_k < \alpha_k$. Note that, unlike in the Gaussian case, $I(\theta)$ is not a multiple of the negative log-density. Rather, the rate function includes the additional terms $-1 - \log(\theta_k)$ and thus a minimizer of the rate function $\theta^*(z)$ might not maximize the density, i.e., be the most probably point.

Example A.4 (Other non-Gaussian distribution). For other non-Gaussian distributions, it may not be possible to derive an explicit form for the cumulant generating function $S(\eta)$ nor for the rate function $I(\theta)$. As a remedy, one could numerically approximate the rate function and its derivative. Alternatively, if available, one could use a mapping between a Gaussian distribution and the target distribution, and, for the LDT arguments discussed next, absorb that mapping into the definition of the parameter-to-event map F .

Appendix B. Probability estimation using first-order approximation of $\Omega(z)$.

In this approach, we integrate the measure $\mu(\theta)$ on the first-order approximation of the set $\Omega(z)$ to approximate $P(z)$. In the engineering literature, a similar method is known as first-order reliability method (FORM) [18]. We replace $F(\theta)$ with the first-order Taylor expansions of $F(\theta)$ at θ^* , i.e.,

$$(B.1) \quad F^{FO}(\theta) := F(\theta^*(z)) + \langle \nabla_{\theta} F(\theta^*(z)), \theta - \theta^*(z) \rangle,$$

where $F(\theta^*(z)) = z$. Replacing the set $\Omega(z) = \{\theta : F(\theta) \geq z\}$ with $\mathcal{H}(z) := \{\theta : F^{FO}(\theta) \geq z\}$, results in the half-space approximation $\mathcal{H}(z)$ of $\Omega(z)$ defined in (2.8), where \hat{n}^* is the normal direction (parallel to $\nabla_{\theta} F(\theta^*)$). The corresponding first-order approximation of $P(z)$ is

$$(B.2) \quad \begin{aligned} P^{FO}(z) &:= \mu(\mathcal{H}(z)) = \mu(\{\theta : \langle \hat{n}^*(z), \theta - \theta^*(z) \rangle \geq 0\}) \\ &= e^{-I(\theta^*(z))} \int_{-\infty}^{\infty} e^{-\|\eta^*(z)\|s} \|\eta^*(z)\| \mu_{\eta^*(z)}(\mathcal{H}(z) \setminus \mathcal{H}(z, s)) ds, \end{aligned}$$

where the last equality follows from (2.16), $\mu_{\eta^*(z)}$ is the tilted measure (2.3), and $\mathcal{H}(z, s)$ is the set defined in (2.12). If the tilted measure on the strip $\mathcal{H}(z) \setminus \mathcal{H}(z, s)$ is known explicitly, this allows to compute $P^{FO}(z)$.

For a multivariate Gaussian parameter, we can compute $P^{FO}(z)$ explicitly. First, we state an auxiliary result for the standard normal distribution.

Lemma B.1 (Measure of half-space for the standard normal distribution). *Assume given the standard normal parameter $\xi \sim \mathcal{N}(0, I_n)$ in \mathbb{R}^n with measure μ^{SN} , $\xi^* = \|\xi^*\| e_1$ aligned with the first basis vector and the half-space $\tilde{\mathcal{H}}_{\xi^*} := \{\xi : \langle e_1, \xi - \xi^* \rangle \geq 0\}$. Then, the measure $\mu^{SN}(\tilde{\mathcal{H}}_{\xi^*})$ can be computed as*

$$(B.3) \quad \mu^{SN}(\tilde{\mathcal{H}}_{\xi^*}) = (2\pi)^{-1/2} \int_{\|\xi^*\|}^{\infty} e^{-\frac{1}{2}s^2} ds \lesssim (2\pi)^{-1/2} \frac{1}{\|\xi^*\|} e^{-\frac{1}{2}\|\xi^*\|^2},$$

where the asymptotic inequality holds for $\|\xi^*\| \rightarrow \infty$.

Proof. For every $\xi \in \tilde{\mathcal{H}}_{\xi^*}$, we can split ξ into two parts:

$$(B.4) \quad \xi = \xi^* + s e_1 + e_1^{\perp} = (\|\xi^*\| + s) e_1 + e_1^{\perp}, \quad s > 0, \quad e_1^{\perp} \in E_1^{\perp}.$$

Using the orthogonality of e_1 and e_1^{\perp} , and the projection P_n , we find

$$(B.5) \quad \|\xi\|^2 = (\|\xi^*\| + s)^2 + \|e_1^{\perp}\|^2 = (\|\xi^*\| + s)^2 + \|P_n(e_1^{\perp})\|_{\mathbb{R}^{n-1}}^2.$$

Applying Fubini's theorem, the measure of the half-space $\mu^{SN}(\tilde{\mathcal{H}}_{\xi^*})$ becomes

$$(B.6) \quad \begin{aligned} \mu^{SN}(\tilde{\mathcal{H}}_{\xi^*}) &= (2\pi)^{-n/2} \int_{\tilde{\mathcal{H}}_{\xi^*}} e^{-\frac{1}{2}\|\xi\|^2} d\xi = (2\pi)^{-n/2} \int_0^{\infty} \int_{P_n(E_1^{\perp})} e^{-\frac{1}{2}[(\|\xi^*\| + s)^2 + \|P_n(e_1^{\perp})\|_{\mathbb{R}^{n-1}}^2]} dP_n(e_1^{\perp}) ds \\ &= (2\pi)^{-n/2} \int_0^{\infty} e^{-\frac{1}{2}(\|\xi^*\| + s)^2} ds \int_{\mathbb{R}^{n-1}} e^{-\frac{1}{2}\|\zeta\|_{\mathbb{R}^{n-1}}^2} d\zeta = (2\pi)^{-1/2} \int_0^{\infty} e^{-\frac{1}{2}(\|\xi^*\| + s)^2} ds \\ &= (2\pi)^{-1/2} \int_{\|\xi^*\|}^{\infty} e^{-\frac{1}{2}s^2} ds. \end{aligned}$$

This proves the equality in (B.3). The asymptotic estimate follows from

$$(B.7) \quad \begin{aligned} \mu^{SN}(\tilde{\mathcal{H}}_{\xi^*}) &= (2\pi)^{-1/2} \int_0^{\infty} e^{-\frac{1}{2}(\|\xi^*\| + s)^2} ds = (2\pi)^{-1/2} e^{-\frac{1}{2}\|\xi^*\|^2} \int_0^{\infty} e^{-\|\xi^*\|s - \frac{1}{2}s^2} ds \\ &\lesssim (2\pi)^{-1/2} e^{-\frac{1}{2}\|\xi^*\|^2} \int_0^{\infty} e^{-\|\xi^*\|s} ds = (2\pi)^{-1/2} \frac{1}{\|\xi^*\|} e^{-\frac{1}{2}\|\xi^*\|^2}. \end{aligned}$$

Here, we drop the term $-\frac{1}{2}s^2$ because it is dominated by $-\|\xi^*\|s$ for large $\|\xi^*\|$. ■

For the Gaussian parameter $\theta \sim \mathcal{N}(\theta_0, C)$, we apply the affine transformation (4.1) to Lemma B.1 to obtain the explicit form of $P^{FO}(z)$ defined in (B.2).

Theorem B.2 (First-order approximation for general Gaussian distributions). *Assume given a Gaussian parameter $\theta \sim \mathcal{N}(\theta_0, C)$ and the optimizer $\theta^*(z)$ of (2.20). Then, the first-order approximation $P^{FO}(z)$ defined in (B.2) can be computed as*

$$(B.8) \quad P^{FO}(z) = (2\pi)^{-1/2} \int_{\sqrt{2I(\theta^*(z))}}^{\infty} e^{-\frac{1}{2}s^2} ds \lesssim (2\pi)^{-1/2} \frac{1}{\sqrt{2I(\theta^*(z))}} e^{-I(\theta^*(z))},$$

where the asymptotic estimate \lesssim is for $z \rightarrow \infty$.

Proof. Using the affine transformation (4.1) and (4.3), we obtain

$$(B.9) \quad \begin{aligned} \langle \hat{n}^*, \theta - \theta^* \rangle &= \langle \nabla_{\theta} F(\theta^*) / \|\nabla_{\theta} F(\theta^*)\|, \theta - \theta^* \rangle \\ &= \langle A^{-\top} \nabla_{\xi} \tilde{F}(\xi^*) / \|\nabla_{\theta} F(\theta^*)\|, A\xi - A\xi^* \rangle = \frac{\|\nabla_{\xi} \tilde{F}(\xi^*)\|}{\|\nabla_{\theta} F(\theta^*)\|} \langle e_1, \xi - \xi^* \rangle. \end{aligned}$$

Thus, the affine transformation of the half-space $\mathcal{H}(z)$ becomes

$$(B.10) \quad \left\{ \xi : \frac{\|\nabla_{\xi} \tilde{F}(\xi^*)\|}{\|\nabla_{\theta} F(\theta^*)\|} \langle e_1, \xi - \xi^* \rangle \geq 0 \right\} = \tilde{\mathcal{H}}_{\xi^*}(z),$$

i.e., the first-order approximation $P^{FO}(z) = \mu(\mathcal{H}(z)) = \mu^{SN}(\tilde{\mathcal{H}}_{\xi^*})$. Applying Lemma B.1 and (4.2) with $\|\xi^*\| = \sqrt{2I(\theta^*)}$, we obtain

$$(B.11) \quad P^{FO}(z) = \mu^{SN}(\tilde{\mathcal{H}}_{\xi^*}) = (2\pi)^{-1/2} \int_{\sqrt{2I(\theta^*)}}^{\infty} e^{-\frac{1}{2}s^2} ds \lesssim (2\pi)^{-1/2} \frac{1}{\sqrt{2I(\theta^*)}} e^{-I(\theta^*)}. \quad \blacksquare$$

Note that the integral in (B.8) in Theorem B.2 is the CDF of the standard normal, which can be computed using the error function, i.e.,

$$(B.12) \quad \Phi(\alpha) := (2\pi)^{-1/2} \int_{-\alpha}^{\infty} e^{-\frac{1}{2}s^2} ds = \frac{1}{2} \left[1 + \operatorname{erf}\left(\frac{\alpha}{\sqrt{2}}\right) \right] \quad \text{for } \alpha < 0.$$

The right estimate in Theorem B.2 also provides an asymptotic approximation of $P^{FO}(z)$, which suggests that the prefactor is $C_0(z) = (2\pi)^{-1/2} / \sqrt{2I(\theta^*(z))}$. However, the error of this prefactor is not controllable, the asymptotic estimation of the probability we should use is the second-order approximation (4.13), as discussed in subsection 4.1.

Acknowledgments. We appreciate helpful discussions with Randall LeVeque, Marsha Berger, Jonathan Weare, Gregor Gassner and Stefan Ulbrich. We would like to thank the anonymous referees for their thoughtful comments and suggestions that helped us improve our paper.

REFERENCES

- [1] A. ALEXANDERIAN, N. PETRA, G. STADLER, AND O. GHATTAS, *A-optimal design of experiments for infinite-dimensional Bayesian linear inverse problems with regularized ℓ_0 -sparsification*, SIAM Journal on Scientific Computing, 36 (2014), pp. A2122–A2148, <https://doi.org/10.1137/130933381>.

- [2] F. BEAUDUCEL, *Okada: Surface deformation due to a finite rectangular source*, MATLAB Central File Exchange, (2020), <https://www.mathworks.com/matlabcentral/fileexchange/25982-okada-surface-deformation-due-to-a-finite-rectangular-source>.
- [3] N. BLEISTEIN AND R. A. HANDELSMAN, *Asymptotic expansions of integrals*, Courier Corporation, 1986.
- [4] A. BOROVKOV AND B. ROGOZIN, *On the multi-dimensional central limit theorem*, *Theory of Probability & Its Applications*, 10 (1965), pp. 55–62.
- [5] A. BORZI AND V. SCHULZ, *Computational optimization of systems governed by partial differential equations*, vol. 8, SIAM, 2011.
- [6] K. BREITUNG, *Asymptotic approximations for multinormal integrals*, *Journal of Engineering Mechanics*, 110 (1984), pp. 357–366.
- [7] M. BRONIATOWSKI AND A. FUCHS, *Tauberian theorems, Chernoff inequality, and the tail behavior of finite convolutions of distribution functions*, *Advances in Mathematics*, 116 (1995), pp. 12–33.
- [8] J. BUCKLEW, *Introduction to rare event simulation*, Springer Science & Business Media, 2013.
- [9] T. BUI-THANH, O. GHATTAS, J. MARTIN, AND G. STADLER, *A computational framework for infinite-dimensional Bayesian inverse problems Part I: The linearized case, with application to global seismic inversion*, *SIAM Journal on Scientific Computing*, 35 (2013), pp. A2494–A2523, <https://doi.org/10.1137/12089586X>.
- [10] Y. CHEN, A. KURGANOV, M. LEI, AND Y. LIU, *An adaptive artificial viscosity method for the Saint-Venant system*, in *Recent developments in the numerics of nonlinear hyperbolic conservation laws*, Springer, 2013, pp. 125–141.
- [11] J. K. CULLUM AND R. A. WILLOUGHBY, *Lanczos Algorithms for Large Symmetric Eigenvalue Computations, Vol. 1: Theory*, Progress in Scientific Computing, Birkhäuser-Verlag, Boston, Basel, Berlin, 1985.
- [12] J. C. DE LOS REYES, *Numerical PDE-constrained optimization*, Springer, 2015.
- [13] G. DEMATTEIS, T. GRAFKE, M. ONORATO, AND E. VANDEN-EIJNDEN, *Experimental evidence of hydrodynamic instantons: The universal route to rogue waves*, *Phys. Rev. X*, 9 (2019), p. 041057, <https://doi.org/10.1103/PhysRevX.9.041057>.
- [14] G. DEMATTEIS, T. GRAFKE, AND E. VANDEN-EIJNDEN, *Rogue waves and large deviations in deep sea*, *Proceedings of the National Academy of Sciences*, 115 (2018), pp. 855–860.
- [15] G. DEMATTEIS, T. GRAFKE, AND E. VANDEN-EIJNDEN, *Extreme event quantification in dynamical systems with random components*, *SIAM/ASA Journal on Uncertainty Quantification*, 7 (2019), pp. 1029–1059.
- [16] A. DEMBO AND O. ZEITOUNI, *Large Deviations Techniques and Applications*, Applications of mathematics, Springer, 1998.
- [17] O. DITLEVSEN AND H. O. MADSEN, *Structural reliability methods*, vol. 178, Wiley New York, 1996.
- [18] X. DU AND W. CHEN, *A most probable point-based method for efficient uncertainty analysis*, *Journal of Design and Manufacturing automation*, 4 (2001), pp. 47–66.
- [19] P. DUPUIS AND H. WANG, *Importance sampling, large deviations, and differential games*, *Stochastics and Stochastic Reports*, 76 (2004), pp. 481–508, <https://doi.org/10.1080/10451120410001733845>.
- [20] M. FARAZMAND AND T. P. SAPSIS, *A variational approach to probing extreme events in turbulent dynamical systems*, *Science Advances*, 3 (2017), p. e1701533.
- [21] H. O. FATTORINI, *Infinite dimensional linear control systems: the time optimal and norm optimal problems*, Elsevier, 2005.
- [22] T. FUJIWARA, S. KODAIRA, T. NO, Y. KAIHO, N. TAKAHASHI, AND Y. KANEDA, *The 2011 Tohoku-Oki earthquake: Displacement reaching the trench axis*, *Science*, 334 (2011), pp. 1240–1240, <https://doi.org/10.1126/science.1211554>.
- [23] D. GAO, K. WANG, T. L. INSUA, M. SYPUS, M. RIEDEL, AND T. SUN, *Defining megathrust tsunami source scenarios for northernmost Cascadia*, *Natural Hazards*, 94 (2018), pp. 445–469.
- [24] M. GILES AND S. ULBRICH, *Convergence of linearized and adjoint approximations for discontinuous solutions of conservation laws. part 2: Adjoint approximations and extensions*, *SIAM Journal on Numerical Analysis*, 48 (2010), pp. 905–921.
- [25] R. GRIESSE, *Parametric sensitivity analysis in optimal control of a reaction diffusion system. I. Solution differentiability*, *Numerical Functional Analysis and Optimization*, 25 (2004), pp. 93–117, <https://doi.org/10.1081/NFA-120034120>.
- [26] W. W. HAGER, *Runge-Kutta methods in optimal control and the transformed adjoint system*, Nu-

- merische Mathematik, 87 (2000), pp. 247–282.
- [27] S. HAJIAN, M. HINTERMÜLLER, AND S. ULBRICH, *Total variation diminishing schemes in optimal control of scalar conservation laws*, IMA Journal of Numerical Analysis, 39 (2019), pp. 105–140.
- [28] N. HALKO, P. G. MARTINSSON, AND J. A. TROPP, *Finding structure with randomness: Probabilistic algorithms for constructing approximate matrix decompositions*, SIAM Review, 53 (2011), pp. 217–288.
- [29] J. S. HESTHAVEN AND T. WARBURTON, *Nodal discontinuous Galerkin methods: algorithms, analysis, and applications*, Springer Science & Business Media, 2007.
- [30] M. HINZE, R. PINNAU, M. ULBRICH, AND S. ULBRICH, *Optimization with PDE Constraints*, Springer, 2009.
- [31] H. KAHN AND A. W. MARSHALL, *Methods of reducing sample size in Monte Carlo computations*, Journal of the Operations Research Society of America, 1 (1953), pp. 263–278.
- [32] K. KUNISCH AND A. RUND, *Time optimal control of the monodomain model in cardiac electrophysiology*, IMA Journal of Applied Mathematics, 80 (2015), pp. 1664–1683, <https://doi.org/10.1093/imamat/hxv010>.
- [33] O. LE MAÎTRE AND O. M. KNIO, *Spectral methods for uncertainty quantification: with applications to computational fluid dynamics*, Springer Science & Business Media, 2010.
- [34] R. J. LEVEQUE, *Finite Volume Methods for Hyperbolic Problems*, Cambridge University Press, 2002.
- [35] R. J. LEVEQUE AND D. L. GEORGE, *High-resolution finite volume methods for the shallow water equations with bathymetry and dry states*, in *Advanced numerical models for simulating tsunami waves and runup*, World Scientific, 2008, pp. 43–73.
- [36] R. J. LEVEQUE, K. WAAGAN, F. I. GONZÁLEZ, D. RIM, AND G. LIN, *Generating random earthquake events for probabilistic tsunami hazard assessment*, in *Global Tsunami Science: Past and Future*, Volume I, Springer, 2016, pp. 3671–3692.
- [37] J. S. LIU, *Monte Carlo strategies in scientific computing*, Springer Science & Business Media, 2008.
- [38] C. MASCIA AND F. ROUSSET, *Asymptotic stability of steady-states for Saint-Venant equations with real viscosity*, in *Analysis and simulation of fluid dynamics*, Springer, 2006, pp. 155–162.
- [39] J. NOCEDAL AND S. WRIGHT, *Numerical optimization*, Springer Science & Business Media, 2006.
- [40] Y. OKADA, *Surface deformation due to shear and tensile faults in a half-space*, Bulletin of the seismological society of America, 75 (1985), pp. 1135–1154.
- [41] R. RACKWITZ, *Reliability analysis – a review and some perspectives*, Structural Safety, 23 (2001), pp. 365–395.
- [42] V. RAO AND M. ANITESCU, *Efficient computation of extreme excursion probabilities for dynamical systems*, arXiv preprint arXiv:2001.11904, (2020).
- [43] T. P. SAPSIS, *New perspectives for the prediction and statistical quantification of extreme events in high-dimensional dynamical systems*, Philosophical Transactions of the Royal Society A: Mathematical, Physical and Engineering Sciences, 376 (2018), p. 20170133.
- [44] T. P. SAPSIS, *Output-weighted optimal sampling for Bayesian regression and rare event statistics using few samples*, Proceedings of the Royal Society A, 476 (2020), p. 20190834.
- [45] G. I. SCHUËLLER AND R. STIX, *A critical appraisal of methods to determine failure probabilities*, Structural Safety, 4 (1987), pp. 293–309.
- [46] G. M. TORRIE AND J. P. VALLEAU, *Nonphysical sampling distributions in monte carlo free-energy estimation: Umbrella sampling*, Journal of Computational Physics, 23 (1977), pp. 187–199.
- [47] F. TRÖLTZSCH, *Optimal control of partial differential equations: theory, methods, and applications*, vol. 112, American Mathematical Soc., 2010.
- [48] S. ULBRICH, J. M. SCHMITT, P. SCHÄFER AGUILAR, AND M. MOOS, *On the numerical discretization of optimal control problems for conservation laws*, (2019).
- [49] E. VANDEN-EIJNDEN AND J. WEARE, *Rare event simulation of small noise diffusions*, Communications on Pure and Applied Mathematics, 65 (2012), pp. 1770–1803.
- [50] S. S. VARADHAN, *Large deviations and applications*, vol. 46, SIAM, 1984.
- [51] C. B. VREUGDENHIL, *Numerical methods for shallow-water flow*, vol. 13, Springer Science & Business Media, 2013.
- [52] S. WAHAL AND G. BIROS, *BIMC: The Bayesian inverse Monte Carlo method for goal-oriented uncertainty quantification. Part i*, arXiv preprint arXiv:1911.00619, (2019).
- [53] L. C. WILCOX, G. STADLER, T. BUI-THANH, AND O. GHATTAS, *Discretely exact derivatives for hyper-*

abolic PDE-constrained optimization problems discretized by the discontinuous Galerkin method,
Journal of Scientific Computing, 63 (2015), pp. 138–162.